

A LOW-COST MOBILE MANIPULATOR FOR INDUSTRIAL AND RESEARCH APPLICATIONS

by

EDWARD VENATOR

Submitted in partial fulfillment of the requirements

for the degree of Master of Science

Department of Electrical Engineering and Computer Science

CASE WESTERN RESERVE UNIVERSITY

August, 2013

CASE WESTERN RESERVE UNIVERSITY
SCHOOL OF GRADUATE STUDIES

We hereby approve the thesis of

Edward Venator

candidate for the degree of **Master of Science***.

Committee Chair

Dr. Gregory Lee

Committee Member

Dr. Murat Cenk Cavusoglu

Committee Member

Dr. Roger Quinn

Date of Defense

April 25, 2013

*We also certify that written approval has been obtained
for any proprietary material contained therein.

Contents

List of Tables	iv
List of Figures	v
Abstract	vii
1 Introduction	1
2 Industrial Mobile Manipulation	4
3 ABBY—System Design	7
3.1 Invacare Ranger Wheelchair Base	7
3.2 ABB IRB-120 Robotic Arm	9
3.3 End Effector	9
3.4 Custom Frame Design	11
3.5 Power	14
3.6 Computing Hardware	18
3.7 Robot Operating System	21
3.8 The Robot Model	22
3.9 Hardware Drivers	24
4 Experimental Software	28
4.1 Mobile Base Planning	28

4.1.1	Localization	29
4.1.2	Mobile Base Trajectory Planning	33
4.2	Inverse Kinematics Solver	35
4.3	Arm Navigation	38
4.3.1	Collision Detection	38
4.3.2	Kinect Data Filtering	39
4.4	Tabletop Box Manipulation	40
4.4.1	Box Manipulation	41
4.5	Calibration	42
4.6	QR Code Recognition and 3D Localization	43
5	Industrial Safety	47
5.1	Reflexive Collision Avoidance	47
5.2	Emergency Stop System	48
5.2.1	E-Stop Systems Used in This Lab	48
5.2.2	E-Stop Requirements	49
6	Validation Results	53
6.1	Localization	53
6.2	Validation Tasks	55
6.3	Battery Performance	61
6.4	The Kinect	63
6.4.1	For Object Localization and Arm Planning	63
6.4.2	For Reading QR Codes	64
7	Conclusion	65
8	Future Work	68
A	Bill of Materials	70

B Revised Emergency Stop Design	72
C Reflexive Collision Avoidance	75
C.1 Reflexive Halt Methods for Mobile Bases	75
C.2 Reflexive Halting for Manipulators	76

List of Tables

6.1	Ten meter odometry test	54
6.2	One meter radius circle odometry test	55
6.3	Results of drive base validation tests	56
6.4	Results of object recognition and manipulation tests	58
6.5	Validation Task Results	60
A.1	Bill of Materials	70

List of Figures

3.1	An annotated rendering of ABBY showing several major components.	8
3.2	The electrical circuit to control the pneumatic gripper using an Arduino microcontroller and a pneumatic solenoid valve.	11
3.3	ABBY, a mobile industrial manipulator.	12
3.4	A block diagram of the power distribution system on the robot	14
3.5	13.8 volt rail dropout when compressor turns on (before addition of filter).	16
3.6	13.8 volt rail during compressor turn-on after addition of an LC filter.	16
3.7	A block diagram of the sensors and computing hardware on ABBY, showing all data connections	17
3.8	A side view of the robot, showing the Kinect's field of view	18
3.9	A close-up view of the Kinect mounted to the robot, showing the mounting bracket	18
3.10	ABBYs robot model, LIDAR data (green points), and Kinect point cloud (multicolored points) visualized in Rviz	27
4.1	The map, odometry, and base frames of the robot localization system.	33
4.2	A histogram of the number of iterations required for the KDL inverse kinematics solver to solve for achievable pose requests.	37
4.3	The box manipulation pipeline	45

4.4	QR Level 3 code	46
4.5	A box localized using the QR code.	46
5.1	Schematic of the emergency stop remote tested on ABBY.	50
5.2	Schematic of the emergency stop receiver and aggregator on ABBY .	51
6.1	Manipulation test results	58
6.2	Voltage curve during battery discharge test with actuators idle . . .	62
6.3	Voltage curve during battery discharge test with drivetrain exercised .	63
6.4	Voltage curve during battery discharge test with arm exercised . . .	64
B.1	Revised emergency stop remote circuit.	72
B.2	Revised emergency stop receiver/aggregator circuit.	73

A Low-cost Mobile Manipulator for Industrial and Research Applications

Abstract

by

EDWARD VENATOR

ABBY is a mobile industrial manipulator, a mobile robot equipped with an industrial robotic arm. The goal in creating this robot was to demonstrate that a robust research platform for mobile industrial manipulation can be created quickly at low cost. This goal was achieved by leveraging commercially-available mass produced hardware and open source software.

The resulting mobile manipulator incorporates a suite of commercially-available sensors and processing hardware to enable the robot to operate as an intelligent agent alongside humans. The robot demonstrated its abilities by performing simple navigation and manipulation tasks in a laboratory setting, and will soon be employed in research on autonomous kitting in industrial environments.

Chapter 1

Introduction

Robots have been an important part of the manufacturing industry for many years. Industrial manipulators are used for tasks such as painting, welding, and assembly. Automated vehicles in industry are used to deliver pallets and other goods through factories and warehouses. However, the combination of these technologies, the mobile manipulator, has yet to see adoption in industry. In academia, researchers have done extensive work toward developing mobile robots, including mobile manipulators. These robots are increasingly capable, demonstrating advanced perception, navigation, and manipulation, as well as a facility for numerous everyday tasks. However, these mobile manipulators have yet to make the jump to industry.

Manufacturers have yet to adopt mobile manipulation robots in spite of the fact that a mobile manipulator has many uses in manufacturing. Mobile manipulators can perform the same tasks as existing industrial manipulators on assembly lines, but they can be relocated to rapidly reconfigure the manufacturing cell, just as human workers can be reassigned as demand changes. In addition, a mobile manipulator can build upon the capabilities of automated vehicles in a factory setting. Whereas automated vehicles must still be loaded and unloaded by human workers, a mobile manipulator can function independently without human assistance. Conversely, recent advances

in robotics allow for closer collaboration than ever before between man and machine. Whereas most industrial robots operate in guarded manufacturing cells, developments in sensing and planning technologies allow robots to operate safely without guards. This opens the door to a mobile industrial robot that can work with human workers as an assistant, rather than a tool.

One of the un-automated tasks in factories is kitting, the task of collecting the components of an assembly from a factory's inventory. Currently, this task is performed by human pickers, sometimes with the aid of vehicles or moving inventory systems. In order for a robot to be able to perform this task, it must be able to navigate a factory environment, recognize and manipulate a variety of objects, and interact with human workers. These requirements add up to the need for a mobile industrial manipulator with modern perception and planning software.

Currently, there are no low-cost mobile industrial manipulators. The lack of an affordable mobile industrial manipulator hampers researchers, who are often budget-constrained, and industrial roboticists, who must justify the cost-effectiveness of the technology they use. In this project, a mobile industrial manipulator was created from commercially available off-the-shelf parts for under \$40,000 (See Appendix 1: Bill of Materials). This is much cheaper than existing mobile manipulators. Unlike experimental hardware, commercially available components are well-tested and exploit economies of scale to reduce costs. As a result, this robot is both robust and affordable.

This robot, called ABBY, was programmed using open source software, including Robot Operating System (ROS). The use of open source software enabled rapid development of simple mobility, manipulation, perception, and planning abilities. In addition, a new ROS interface for the industrial robotic arm on ABBY was created as part of this project. The ROS interface was the first ROS drive for ABB robotic arms. The code for this interface was contributed to the ROS Industrial project, and

it serves as the basis of that project's recently-released ABB robotic arm driver.

ABBY demonstrated the navigation and manipulation capabilities necessary to the kitting task by performing simple tasks. The robot can localize accurately within its environment and navigate to a specified position. Presented with manipulable objects on a table, the robot can locate them, pick them up, and store them in an onboard carrier. These tasks are significant because they form the basis of the kitting task. By completing these tasks, the robot has demonstrated the necessary capabilities to perform kitting.

Chapter 2

Industrial Mobile Manipulation

Mobile industrial robot development began with Automated Guided Vehicles (AGVs). AGVs are unintelligent vehicles employed to move loads in factories following paths that were marked with wires buried in the factory floor. These vehicles were only practical for permanent installations in unchanging environments; “reprogramming” a first generation AGV required that the path be removed from the floor and reinstalled [1].

More modern AGVs have eschewed physically-marked paths in favor of virtually-defined paths. The AGV uses sensor systems to localize itself in the factory and navigation software to follow paths, which can be statically defined or dynamically chosen by a higher-level planner. The higher level planner chooses paths for the AGV from amongst a graph of paths through the factory or warehouse. A single high-level planner may coordinate multiple AGVs to prevent traffic jams and allocate tasks [2]. Although these modern AGV systems are more flexible than their predecessors, they still depend on an ordered factory or warehouse environment, and are not designed to cooperate with human workers. They execute pre-programmed routines to move loads between loading docks.

Implementing such a system requires that all of the possible paths for the AGVs be

predefined, which makes commissioning such a system a lengthy and labor-intensive process. Predefining all of the paths for an AGV may not be practical if the inventory system is large and does not have readily-defined nodes such as loading docks. AGV systems are useful for tasks such as pallet transportation, and many such systems are forklifts [3]. However, AGVs are inflexible; they cannot adapt to changing inventory organization, changing assembly line configurations, or changes in their environment. An obstacle placed along an AGV path could disable an entire AGV system by creating a bottleneck or blockage.

Kiva Systems, a producer of automated inventory systems, has moved beyond the AGV paradigm to a smart-warehouse system [4]. In this type of system, all of the inventory is stored on pallet-like mobile shelves, and a group of mobile drive units rearrange and deliver the shelves as necessary to bring items to assembly and packing stations. Kiva robots cannot manipulate individual items, so the task of loading and unloading the shelves is left to human pickers, and the robots are used purely as mobile bases for the shelves. This system is an evolution from the traditional AGV in that there are no pre-planned paths; instead, the mobile robots are entirely free to move through the warehouse environment. This system also has another advantage over AGV systems that stems from the entire inventory being movable. Namely, the warehouse is constantly being reorganized as it is used, moving items around to make commonly-needed items more accessible and improve the speed of the overall system [5]. Although the Kiva system does not require prelaid or preplanned paths, it does require that a warehouse be specifically designed for and used exclusively by its robots. The system cannot be used with existing inventory shelves, only with the movable shelves designed for its robots. It also requires that the inventory environment be outfitted with a grid of barcodes on the floor to facilitate localization.

Mobile manipulators have made little headway in industry, partly because of the rarity and cost of mobile manipulators [6]. However, researchers have been exploring

the application of mobile manipulators in industrial settings for several years. In 2004, a group at the University of Verona, Italy devised a mobile manipulator for the pharmaceutical industry [7]. This robot consisted of a custom-made 5 DOF manipulator with one passive DOF mounted on top of a commercially-available mobile base. The system used a vacuum gripper to pick up cardboard boxes from pallets and put them on shelves. This system was capable of navigating freely through a partially structured dynamic environment using a local and global planner. The resulting robot is functionally similar to ABBY, but was to be used for the task of loading items from pallets into an inventory shelving system, whereas ABBY's purpose is to pick from inventory and deliver items to assembly stations.

More recently, in 2011 a group at the Intelligent Systems and Production Engineering Research Center for Information Technology in Karlsruhe, Germany developed a bimanual manipulator using a custom drive base and two KUKA Lightweight Robot arms [8]. It used a Microsoft Kinect, two high resolution cameras, and three LIDAR scanners for perception, as well as force feedback in its manipulators. This platform was exceptionally capable, but was designed more as a general-purpose mobile manipulator than as an industrial robot. This platform's price was not listed, but is substantially more than the cost of ABBY. The main focus of the project was on the development of a software platform for mobile manipulation and on developing new planning methods for the robot's manipulators.

Chapter 3

ABBY—System Design

ABBY's design was dictated by several factors. The primary factor in the design was reduction of cost, which was achieved by using materials and components already available in Case Western Reserve University's Mobile Robotics Lab.

3.1 Invacare Ranger Wheelchair Base

The Invacare Ranger is a wheelchair chassis in Invacare's Storm series. The wheelchair base has a differential drive system with two pneumatic drive wheels in the back and two solid caster wheels in the front. The drive wheels are each powered by a 24 volt DC motor geared for a maximum speed of 5 miles per hour (2.24 m/sec) [9]. Because of the configuration of the robot's wheels, it can spin on its own axis and drive forward and backward. It cannot move sideways.

The Invacare motor control electronics have been replaced with a Sabertooth 2x50 dual brushed DC motor controller. The Sabertooth 2x50 is an H-bridge PWM motor controller that supplies a variable DC voltage from -24 volts to +24 volts to each motor based on commands it receives over a serial data connection. The Sabertooth 2x50 is powered by a 24 volt DC rail that is energized and de-energized by the emergency stop circuit described in Section 5.2.

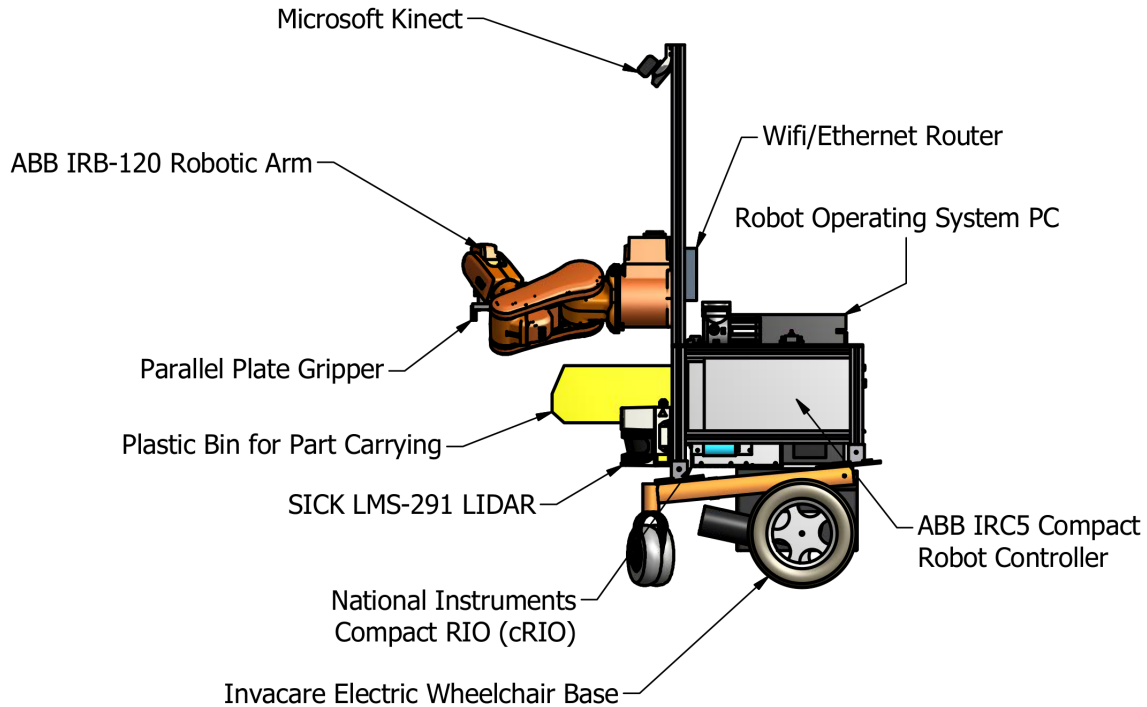


Figure 3.1: An annotated rendering of ABBY showing several major components.

©2013 IEEE [9]

The wheelchair base is prone to wheel slip when commanded to accelerate or decelerate quickly. The acceleration limits of the robot were characterized by testing a series of constant linear acceleration commands. These tests were performed with the robot's arm in the stowed position on a smooth tile floor. From these tests, the maximum achievable forward acceleration (with no slip) was determined to be about $.1 \text{ m/sec}^2$ on tile floor. The same test was performed using constant rotational accelerations. From these tests, the maximum rotational acceleration was determined to be about 0.1 rad/sec^2 on tile floor.

3.2 ABB IRB-120 Robotic Arm

The manipulator on the robot is an ABB IRB-120 industrial robotic arm [10]. The IRB-120 is a six-axis robotic arm with a spherical wrist. It has a tool flange that allows for the mounting of end effectors as well as pneumatic and electrical connections near the tool flange to connect sensors and actuators to the arm. The IRB-120 is ABB’s smallest robotic arm, with a 580 mm reach and a payload capacity of 3 kg. The arm itself weighs 25 kg and is mounted to the extreme front of the robot, which means its weight exerts a large moment on the robot. This was a serious consideration in the placement of the robot’s center of mass. The arm can be mounted at any angle, and on this robot is mounted at 90° (with the base mounted to a vertical surface). The arm is mounted vertically on the front of the robot so that the majority of the arm’s work envelope is outside of the volume of the robot. This maximizes the functional work envelope of the arm and minimizes the possibility of the arm colliding with other parts of the robot. However, this mounting orientation does somewhat hamper the arm’s ability to lift objects from horizontal surfaces.

The IRB-120’s joints are powered by non-back-drivable AC electric servos, with position feedback from resolvers. According to ABB, the IRB-120 is capable of position repeatability of 10 micrometers [10]. The arm’s position is controlled by an ABB IRC5 Compact robot controller, which is in turn commanded through the ROS Industrial interface. The details of this control structure are described in Section 3.9.

3.3 End Effector

There are many types of grippers and graspers used with industrial robots. Some are purpose-built fixtures for holding specific parts. Other grippers use suction to be able to quickly pick up light objects such as electronic components. Still others use dexterous fingers to be able to securely pick up and manipulate objects of different

shapes and sizes. This robot uses one of the simplest gripper types, a two-position parallel plate gripper.

The gripper was primarily chosen based on cost and availability. A dexterous grasper like the BarrettHand costs about \$30k, which would nearly double the cost of this robot. The pneumatically-actuated parallel plate gripper has only two positions (open and closed), and is simply and cheaply constructed from aluminum and a single double-throw pneumatic piston. When open, the gap between the jaws is 53 millimeters, and when closed the gap is 35 millimeters. The insides of the jaws are lined with high-friction conveyor belt material.

The gripper is pneumatically actuated using stored air from accumulator tanks that are kept at 825 kPa by an onboard compressor. The compressor is turned on and off by an Innovation First Spike relay, which is controlled by a digital pressure switch calibrated to turn the compressor on at 690 kPa and turn it off at 825 kPa. This control circuit can be seen in the power distribution diagram in Figure 3.4. The 825 kPa stored air is regulated down to 275 kPa working pressure and used to actuate the gripper. The pneumatic piston in the gripper is controlled by a pneumatic solenoid valve, a magnetically actuated valve with one pressure inlet and two pressure outlets. The inlet is connected to the regulator, and the outlets are connected to the gripper's pneumatic piston so that applying pressure through one outlet opens the gripper and applying pressure through the other outlet closes the gripper. The solenoid valve is designed so that when one outlet is connected to the pneumatic pressure inlet, the other is vented to the atmosphere. The valve is actuated by running current through a solenoid coil. The solenoid coil is controlled by a custom circuit based on an Arduino microprocessor development kit, as shown in Figure 3.2.

Although the gripper has only two positions, the pneumatic nature of the system makes the gripper jaws back-drivable, with a constant gripping force proportional to the working pressure of the pneumatic system, which was set by the pneumatic

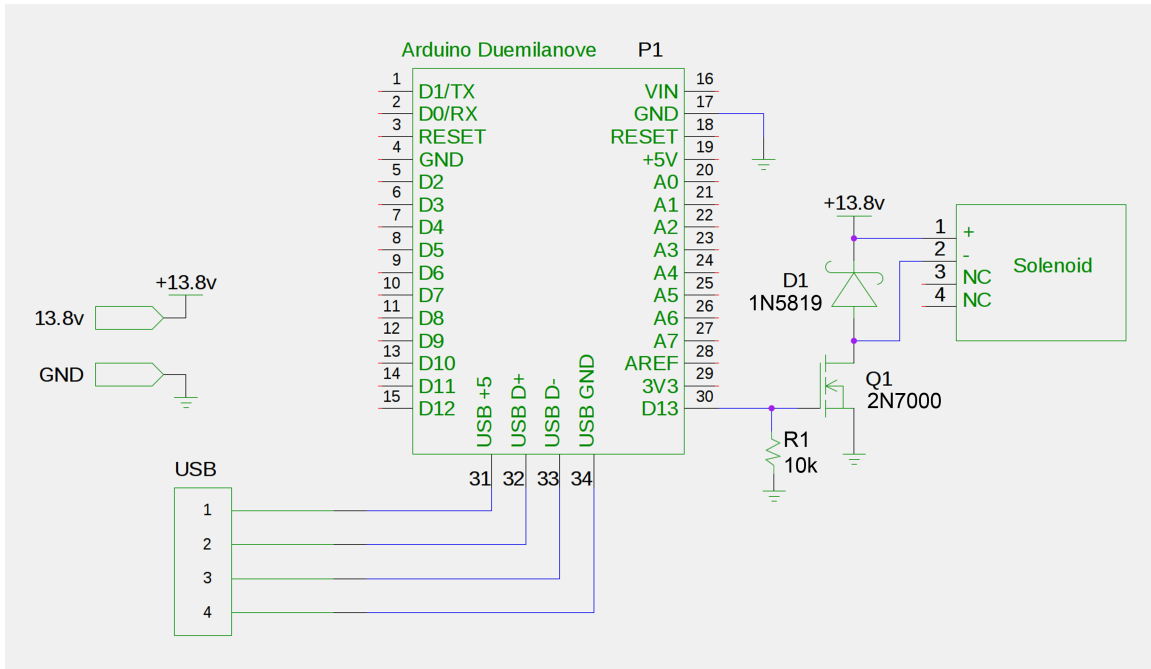


Figure 3.2: The electrical circuit to control the pneumatic gripper using an Arduino microcontroller and a pneumatic solenoid valve.

system's adjustable regulator to 275 kPa. The regulator can be set to any pressure up to the system's maximum pressure of 825 kPa. The working pressure was chosen so that the gripping force would be great enough to ensure a strong grasp on manipulated objects without being so great as to damage them.

3.4 Custom Frame Design

Coupling together the ABB IRB-120 robotic arm and the Invacare Ranger wheelchair base is the main frame of the robot. The structural elements of the frame are made from Bosch Rexroth aluminum profile struts. Bosch rail is an extruded aluminum product with T-slots running the length of the rail. It has several features that make it a good choice for a prototype robot. Because Bosch rail is aluminum, it is easy to machine, but strong and relatively light. Because T-slots do not require holes to be drilled in the rail for mounting, the robot can be easily reconfigured without

remachining frame members. However, heavy objects mounted to vertical rails, such as the arm, may slip if the bolts are not very tight.



Figure 3.3: ABBY, a mobile industrial manipulator.

©2013 IEEE [9]

The frame is designed to hold the IRC5 Compact robot controller and the assorted power and control electronics of the robot. The IRC5 is large (480mm x 580mm x 258mm) and heavy (28.5kg), and it dominates the robot frame. The robot frame was meticulously designed in 3D CAD software to place the center of mass as close to the center of the robot volume as possible to prevent tipping. The mass of every component of the robot was entered into the CAD models, and components were placed so as to keep the center of mass low as well as relatively centered between the

front and rear wheels. The final center of mass, as determined by the CAD model, is 0.2 meters in front of the rear wheels (0.48 meters behind the front wheels) and 0.494 meters from the ground. The robot’s estimated weight is 195 kg.

On the front of the frame is a vertical mast made of Bosch rail. This mast serves several purposes. First and foremost, it provides a mounting point for the IRB-120 robotic arm. The rails are spaced so that the arm’s four mounting holes line up with the two rails, and the arm can be fixed to any position along the height of the rail by tightening the T nuts that hold it in place. This allows the robot to be reconfigured for different tasks that may require the arm to be mounted at different heights. In addition to holding the arm, the mast provides a high vantage point for the Kinect camera and allows the WiFi router to be mounted far away from possible interference from other electronics.

In addition to the Bosch rail structural elements, the frame includes four panels for mounting the robot’s electronic and pneumatic components. It was important to protect the onboard electronics from damage in the case of a collision, so the majority of the electronics are mounted to a polycarbonate panel underneath the IRC5, where they are completely enclosed inside the robot. This keeps the electronics safe from collisions, and the mass of the heavy power electronics is kept low to the ground. Although this design is advantageous in terms of keeping the robot’s overall volume small and the robot’s center of mass low, it is not user-friendly in the rare event that these components require service.

The top panel of the robot, also made of polycarbonate, holds the pneumatic system and the PC. These were mounted on the top panel in anticipation that they would require more user access and to put the pneumatics close to the arm. Two front panels, made of aluminum sheet, hold the main power distribution rail and the power supply for the LIDAR. The power distribution rail is mounted on a front panel to make it easily accessible, and the LIDAR power supply is mounted on a front panel

to place it close to the LIDAR, which is mounted to the front frame rail.

3.5 Power

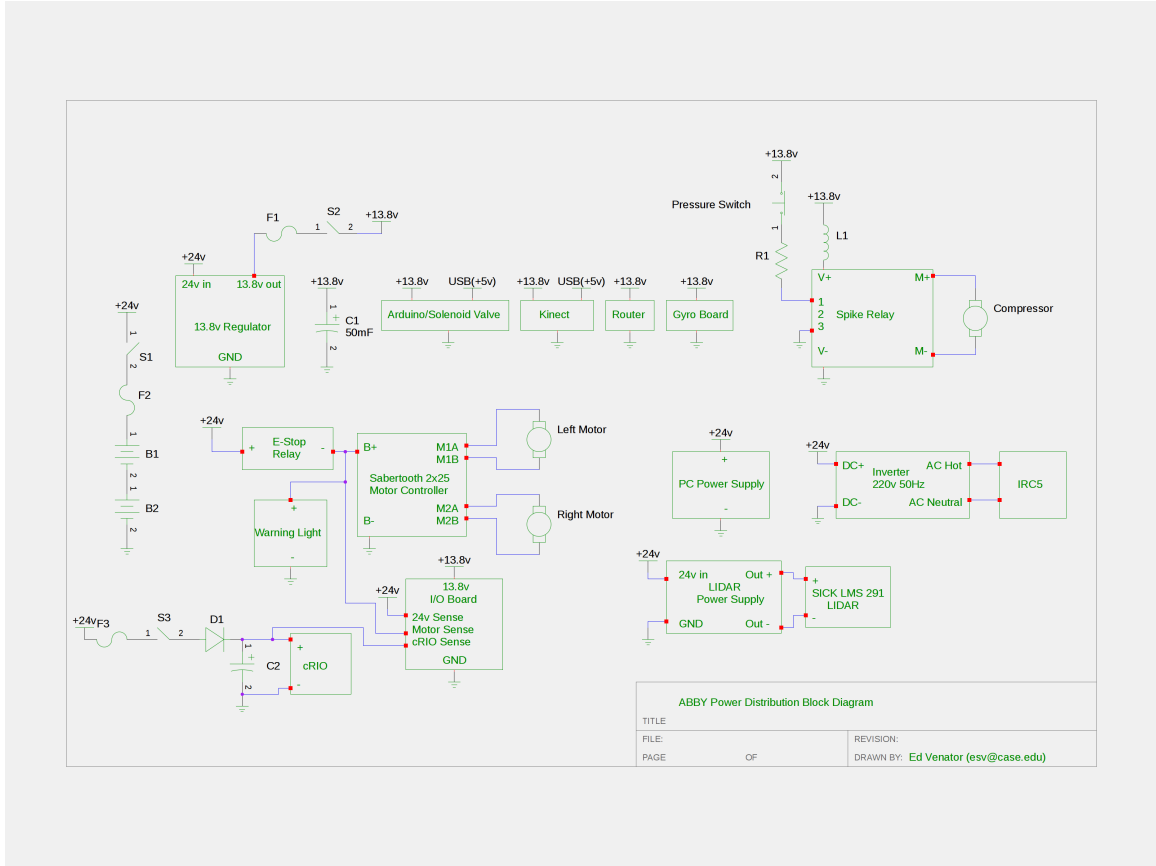


Figure 3.4: A block diagram of the power distribution system on the robot

All of the robot's power is distributed using DIN rail power distribution blocks. These blocks are modular, insulated, and compact. The robot has two DC voltage buses (24 volt DC, and 13.8 volt DC) and a single ground block. In addition to these main voltage buses, several parts of the robot have their own power regulators and supplies.

The robot's main voltage rail is a 24 volt DC bus supplied by two 12 volt batteries in series. This 24 volt bus is required by the Invacare wheelchair base's drive system, and the Invacare wheelchair base includes the batteries that supply the bus. The

batteries are protected by a 120 amp resettable circuit breaker, which also serves as the main power switch for the robot. In addition to the robot’s drivetrain, the robot’s PC, LIDAR, and the National Instruments cRIO are all powered directly from the 24 volt DC bus.

Because the cRIO is a critical component of the drivetrain and the inductive kick of the motors can cause significant noise on the 24 volt DC bus, a peak-detector circuit is used to protect the cRIO from voltage fluctuations on the 24 volt rail.

In addition to the two DC buses on the robot, there is an AC inverter, which is used to power the ABB IRC5 Compact robot controller. The IRC5 requires 220 volt AC at 50 Hz. The inverter is capable of delivering up to 2 kW of power continuously and surges of up to 3kW, which is necessary to account for the high current draw when the controller first enables the motor drive. The inverter is powered from the 24 volt DC bus and is only used to power the IRC5 Compact and (through the IRC5) the IRB-120 robotic arm.

Much of the electronics on the robot requires a lower voltage to operate, nominally 12 volts DC. These electronics are powered by a Samlex America SDC-15, a 13.8 volt switch-mode step-down regulator that can supply up to 12 amps [11], which is powered from the main 24 volt bus. This bus powers the WiFi router, emergency stop circuitry, the cRIO interface board, the Kinect camera, and the pneumatic compressor.

Because the compressor draws a large amount of current, the 13.8 volt regulator’s output would drop to about 5 volts for approximately 450 ms (see Figure 3.5) when the compressor switched on. This droop was sufficient to cause the onboard Ethernet router to reboot, interrupting communications between the computers onboard. In order to prevent this problem, an LC filter was added to the 13.8 volt power rail. A 50mF capacitor acts as a charge reservoir for the electronics on the 13.8 volt power rail, including the router. A 55 H inductor acts as a current choke to limit the instantaneous current draw when the compressor turns on. Figure 3.6 shows that

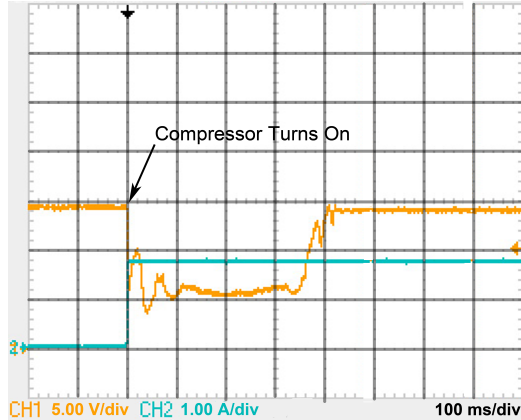


Figure 3.5: 13.8 volt rail dropout when compressor turns on (before addition of filter).

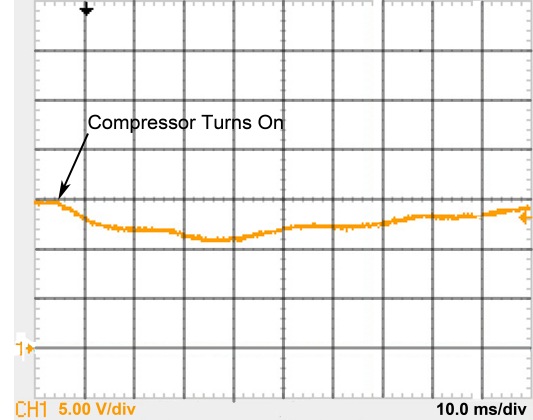


Figure 3.6: 13.8 volt rail during compressor turn-on after addition of an LC filter.

this filter kept the 13.8 volt rail from dropping below 10 volts, and it recovers to its nominal voltage in under 100 ms. This droop is not enough to cause the router to reboot. In order to monitor the state of the voltage rails, each one is connected to an analog to digital converter (ADC) on the National Instruments Compact RIO that controls the drive base (see Section 3.6). The ADC monitors the main 24 volt bus, the 13.8 volt bus, the power supply to the cRIO (which is protected from rail droop by a peak detector, as shown in Figure 3.4), and the rail that powers the drive base, which is switched on and off by the emergency stop circuit.

In order to sense the motor speed, there is a Grayhill 61R-256 encoder on each motor’s output shaft. The encoder outputs quadrature pulses at a frequency proportional to the motor speed. These motor shaft encoders cannot provide accurate wheel position information for odometry because of backlash in the gearboxes. For odometry, there is an encoder attached to each wheel by a toothed belt. The wheel encoders spin sixteen times more slowly than the motor encoders, but still provide a very high resolution output (0.7 mm per encoder tick). The output of the wheel encoders is differentiated to get the wheel velocities, which are then fed as control inputs into a Kalman filter that outputs a robot pose estimate consisting of X and Y

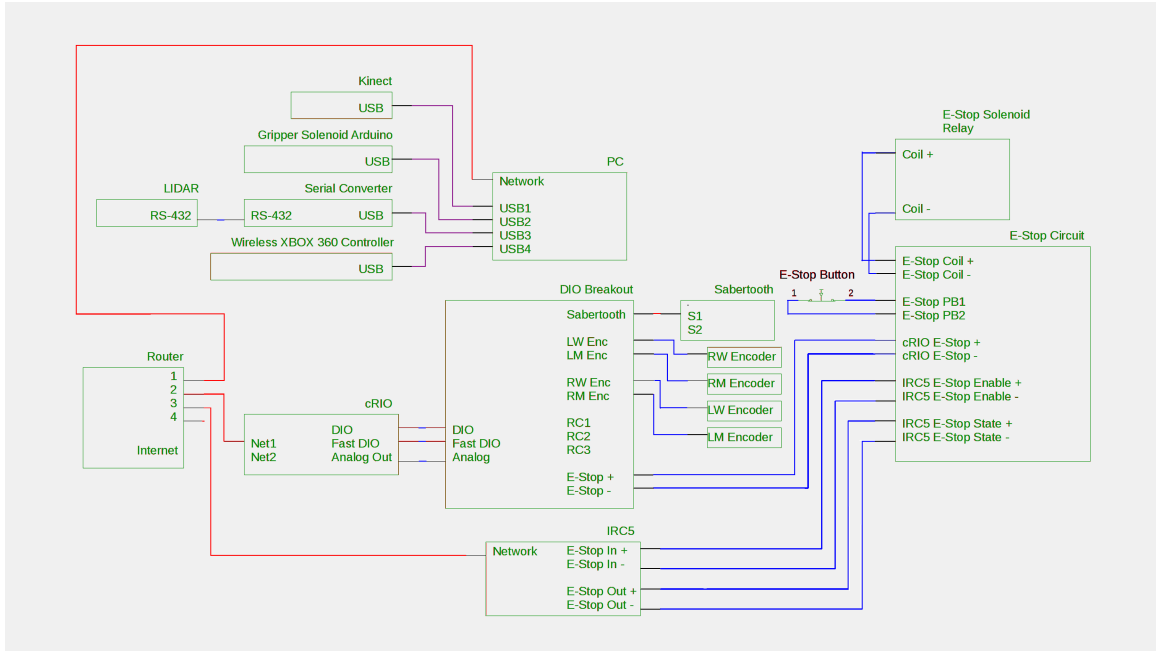


Figure 3.7: A block diagram of the sensors and computing hardware on ABBY, showing all data connections

coordinates and a heading.

The Microsoft Kinect is an RGBD (Red, Green, Blue, Depth) camera marketed as a gaming controller. ABBY has a Kinect camera mounted high on the front mast with a custom-designed acrylic bracket that fixes it at a downward-looking angle of 51 degrees from the horizontal. At this angle, the Kinect is looking down into the IRB-120’s work envelope and capable of viewing the floor in front of the robot. The RGBD data from the Kinect are converted into three-dimensional point clouds, which are used to detect obstacles and manipulable objects.

An LMS-291 laser ranging sensor (LIDAR) from SICK AG of Waldkirch, Germany is mounted horizontally to the front of the robot. The LIDAR provides planar range scans of a 180 degree arc in front of the robot. These range data are used for localization and obstacle detection.

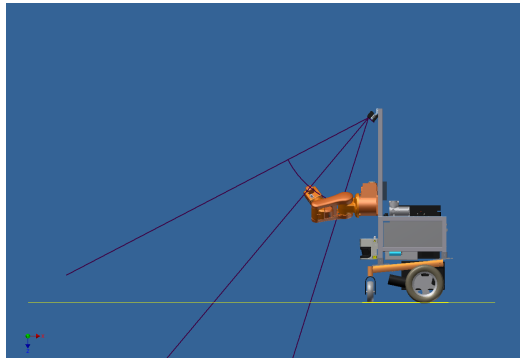


Figure 3.8: A side view of the robot, showing the Kinect’s field of view



Figure 3.9: A close-up view of the Kinect mounted to the robot, showing the mounting bracket

3.6 Computing Hardware

The robot has three main computing devices on board, connected by a local Ethernet network with an onboard WiFi access point so operators can wireless connect to the robot for maintenance and control.

The majority of the robot’s processing is performed on a Linux PC. This PC runs all of the perception and higher level planning algorithms, which do not require a real-time operating system. In addition, the PC is responsible for processing LIDAR and Kinect data directly from the sensors. These tasks are computationally intensive, particularly the tasks of filtering the robot’s links out of the Kinect point cloud and maintaining a collision map.

The computer was specified so as to balance cost, physical size, and processing power. The computer’s motherboard is an ASUS micro-ATX motherboard, which was chosen over the smaller mini-ITX form factor because many mini-ITX boards were found to have poor thermal management during the construction of the autonomous wheelchair OTTO. The case chosen was the smallest micro-ATX case available from major computer vendors, measuring 0.33m x 0.10 m x 0.39 m. The case included a

compact AC power supply, but this was replaced with a 24 volt DC power supply. The PC’s processor is an Intel i5 2500k, a four-core processor utilizing Intel’s Sandy Bridge architecture clocked at 3.2 GHz. The PC also has 8 gigabytes of DDR3 RAM and a solid state hard drive. Combined, the total cost of the PC for the robot was about \$550. A full cost breakdown for the PC, as well as the rest of the robot, can be found in Appendix 1: Bill of Materials.

Some tasks pertaining to sensor interfacing and motor control require real-time processing, analog to digital conversion, and robust digital I/O. These tasks are beyond the reach of commercially-available PC hardware. The cRIO 9072 from National Instruments combines a 266 MHz PowerPC processor with a 1M gate Xilinx FPGA. The PowerPC processor is running the vxWorks real-time operating system and the Xilinx FPGA is connected to the PowerPC processor and to 8 reconfigurable IO slots. These reconfigurable I/O slots accept a myriad of modules sold by National Instruments ranging from analog to digital converters to serial bus interfaces. ABBY’s cRIO is equipped with three IO modules. A digital I/O module is used to read values from the wheel encoders and to output the enable signal to the emergency stop. A high speed digital I/O module is used to read values from the motor encoders and to send serial packets to the Sabertooth motor controller. An analog input module is used to monitor the voltage rails.

The FPGA is used to perform minimal signal processing on the inputs and outputs, including counting encoder ticks and forming packets to command motor speeds. Besides this signal conditioning, the only processing performed on the FPGA is the PID controller that determines the motor speeds. Because PID control is dependent on very fast loop closure (10 ms) and is sensitive to the lag that can occur even in a real-time operating system, it is implemented on the FPGA. In addition to this minimal processing, the FPGA acts as a bridge between the IO connections and the cRIO’s PowerPC processor.

In addition to the FPGA, the robot uses the cRIO’s PowerPC processor for low-level processing related to the operation and control of the drive base. The robot’s physical state observer (PSO) takes in the current encoder counts and uses a Kalman filter to generate an estimate of the robot’s current position. The PSO used on this robot is described in detail in [12]. In addition to this processing, the PowerPC processor relays raw values from the FPGA to the robot’s PC over the robot’s local Ethernet network and receives speed commands from the robot’s PC that it then passes to the PID controller on the FPGA.

The ABB IRB-120 robotic arm is controlled by ABB’s IRC5 Compact robot controller. This controller contains all of the processing hardware and power electronics to control the arm. It runs a proprietary real-time operating system that must be programmed in ABB’s RAPID programming language. Although the IRC5 has built-in software to perform inverse kinematics and path planning, the preferred method of programming it is to “teach” it by manually moving the robot to points. This method is useful in industrial environments where the robot executes a predefined path, but it is not compatible with a dynamic planner.

Because of these limitations of the RAPID programming language and operating system, the majority of the arm planning is performed on the PC, and the software on the controller performs the bare minimum to interface with the IRB-120 arm. There are two TCP servers running on the controller. One publishes the current state of the arm, including joint states, and the other receives joint trajectories from the ROS system on the PC. The only processing that the IRC5 performs is interpolation between the points in the trajectory, which is accomplished with the built-in functions of the RAPID programming language. All higher-level arm planning functions are performed by the PC.

3.7 Robot Operating System

The robot’s software runs within Robot Operating System (ROS). ROS is a framework for research robotics development that encapsulates algorithms as nodes, which pass information to each other through sockets as messages. The use of modular nodes makes it easy to add functionality to the robot without adding complexity. Standardization of messages within ROS makes it easy to swap nodes for other nodes that perform similar functions. ROS also has a vast library of existing nodes and algorithms, allowing researchers to leverage prior work without having to reimplement algorithms.

ROS nodes communicate to each other by sending messages to each other on topics. Messages have predefined types that define the fields of the message. Many message types are already defined in the ROS core and in existing ROS packages, but developers can also define their own message types. Topics are identified by names, which are organized into hierarchical namespaces. ROS nodes can publish messages to one or more topics for other nodes to subscribe to. Many ROS nodes may publish to a single topic, and many ROS nodes can subscribe to a topic. ROS topic communication is distributed, meaning that nodes communicate directly from the publisher to the subscriber, and the ROS master node only facilitates this communication by maintaining a list published topics and negotiating the direct connections between nodes [13].

In addition to communicating through ROS topics, ROS nodes can provide services to one another. A service is defined by a request message and a response message. A ROS node providing a service advertises it to other nodes in a hierarchical namespace. A service client sends a request message to the service server containing parameters or data to be processed. The service server performs the service requested and sends a reply message containing processed data or a status message about the service [13].

ROS also provides an action server interface. Like ROS services, ROS actions are based on a server-client model. Whereas services are synchronous—the client blocks until it receives a reply—actions are asynchronous, making them more appropriate for requests that take a long time, such as moving an actuator or querying a sensor. Actions consist of three messages—a goal, a feedback message, and a result. The client sends a goal message to the action server. The server acknowledges the goal and begins processing it. Optionally, the server may publish feedback messages while it is processing the goal. When the server is finished processing the goal, it sends a result message, which notifies the client that it has finished processing the goal and returns the result of the process [14].

3.8 The Robot Model

Another feature of ROS is the definition of robot physical characteristics using Universal Robot Descriptor Files (URDF). URDFs incorporate kinematic information such as joint geometry, inertial properties, collision information defined by geometric primitives or meshes, and visualization rendering information, also defined by geometric primitives or meshes. URDFs are a dialect of XML, with tags defined for robot links and joints. Various ROS nodes use the data parsed from URDFs for tasks such as kinematics and frame transforms, collision detection, physics simulation, and visualization in the Rviz GUI application. ABBY is fully defined in a modular URDF file generated using the ROS xacro system of XML generation macros.

The robot frame is defined in the URDF as a series of links joined by fixed joints. The visual, collision, and inertial data for each of the links were imported from a 3d model of the robot created in Autodesk Inventor, a 3D CAD package. The only movable joints on the main robot frame are the wheels and casters. When the robot is running, a static joint state publisher publishes a constant angle to all of these

joints, but if the necessary sensors (joint position encoders on the casters) are added, the joints could be used in the future for tasks such as modeling the current position of the casters.

The Kinect and the SICK LIDAR are defined as xacro macros that place their visualization and collisions meshes in the URDF and define all of the necessary sensor frames as mass-less links. This makes it easy to reuse the sensors in models of this and other robots by importing the xacro macros. The macros each define a sensor root link at an externally visible point on the sensor body. This is much easier than the previous method of manually publishing a transform from the robot root link to the sensor frame because the sensor frame is located inside the body of the sensor and consequently difficult to locate on the physical robot.

The IRB-120 arm is also defined as a xacro macro. Each of the seven links is defined by a visualization/collision mesh created from solid models of the arm obtained from ABB. These links are joined by six joints, which are defined according to the joint dimensions and rotation limits provided in documentation from ABB. This definition of the arm is used by the forward and inverse kinematics solvers to convert joint angles into Cartesian coordinates and vice versa. It was also used to generate the arm navigation package that performs trajectory planning for the arm.

In addition to providing the geometric definition of the robot, the robot model makes the Rviz robot visualization GUI much more usable. Because visualization meshes of the robot are defined, Rviz can render an accurate visualization of the robot in its current state. This is useful for verifying that the state of the robot in ROS matches the physical state of the robot. In an industrial environment, it would also allow a user to remotely monitor a robot without the need for a CCTV system external to the robot.

3.9 Hardware Drivers

ROS uses a software driver implemented as a ROS node to read data from a sensor or send commands to an actuator. The driver node for a sensor interfaces with the sensor hardware and publishes data as ROS messages to the appropriate ROS topic(s). The driver node for an actuator subscribes to actuator commands on the appropriate ROS topic and interfaces with the actuator hardware to execute the commands. ABBY’s Kinect camera and SICK LIDAR use preexisting open source drivers [15] [16], and the ROS driver node for the mobile base was developed previously by this lab for other robots using the same hardware, and required limited modification for this robot [17]. The driver for the ABB robotic arm was written for this platform in collaboration with the Southwest Research Institute (SWRI) of San Antonio, Texas as part of the ROS Industrial Project.

The mobile base is controlled by software running on the cRIO, as described in Section 3.6. The cRIO sends data to the PC containing information about the robot’s pose, the state of the power supplies, and raw count data from the encoders. The PC sends angular and translational velocity commands to the cRIO and may send commands to the cRIO to activate or deactivate the emergency stop or to reboot the cRIO. These two tasks (sending and receiving data) are handled by two different ROS nodes. A third ROS node publishes pose information as a standard ROS message.

The receiving ROS node handles UDP packets from the cRIO. Encoder data are checked to ensure that all of the encoders are updating properly, and voltage data are checked to monitor the battery level and health of the power regulator. The results of these checks are fed into a ROS diagnostic updater, which provides feedback to the operator. Voltage information is also published to a custom ROS message so that other nodes on the robot can subscribe to the voltage data. Pose information is published as a custom ROS message type and sent to the odometry translator node. The odometry translator publishes the robot’s pose using ROS-standard odometry

messages, which are used in ROS’s planning and localization packages.

The sending ROS node subscribes to ROS ”twist” topics containing desired rotational and translational velocity from the mobile base trajectory planner and sends the commands to the cRIO as UDP packets. It also provides a ROS service to reboot the cRIO and ROS services to enable and disable the drive base motors with the emergency stop.

The gripper driver is a ROS node that runs natively on an Arduino’s AtMega 328 microcontroller using the ROS Serial framework. It sends and receives ROS messages over the USB serial connection. A ROS node, included in the ROS Serial package, runs on the PC and acts as a transparent bridge between the ROS system and the ROS node on the microcontroller. The ROS node on the microcontroller publishes joint state messages describing the current position of the gripper plates and provides a ROS service to open and close the gripper. The Fuerte version of ROS Serial did not properly support ROS services [18]. In order to implement a service on the Arduino, changes were made to the ROS Serial bridge node and microcontroller code to enable support of services [19].

ABBY uses the ROS Industrial framework of messages and driver nodes to control the IRB-120 using the IRC5 Compact. ROS Industrial is a project led by SWRI to develop a standard ROS framework for using ROS with industrial robots [20]. ABBY’s ROS Industrial driver was written specifically for this project, and has been incorporated into the ROS Industrial codebase.

Part of the ROS Industrial arm driver runs on the IRC5 Compact. The software on the IRC5 Compact is written in RAPID, ABB’s proprietary programming language. The software running on the IRC5 Compact consists of a trajectory server, a state server, and a motion process. The state server periodically polls the positions of the joints in the arm and sends that information to the ROS system. The trajectory server receives trajectory packets from the ROS system and queues them for the motion

process. When the trajectory server receives a complete trajectory, it passes the trajectory to the motion process, which sends the arm to each point in the trajectory. In order to generate smooth motion through the trajectory, the intermediate points in the trajectory are defined as low-precision waypoints. Because RAPID only has fixed-length data structures, trajectories must have a fixed maximum length. Paths generated for the IRB-120 with the current planner software have been experimentally determined not to exceed 300 points in most cases, so the maximum trajectory length was set to 500.

The robotic arm driver, like the mobile base driver, consists of two ROS nodes that communicate with a server running on the IRC5 robot controller. ROS trajectory messages describe the trajectory of a robotic arm as a series of points, with each point describing the position and velocity of all of the robot's joints. One of the ROS nodes subscribes to ROS trajectory messages, breaks them up into packets, and sends them to the IRC5 controller over TCP using a standard packet structure defined by SWRI. The other ROS node connects to the IRC5 controller over TCP and listens for state information from the controller, which is sent using another packet structure defined by SWRI. It publishes this state information, consisting of all of the robot's joint angles, as ROS joint state messages and ROS joint trajectory feedback messages. These messages are used by other ROS nodes to determine the position of the robot's arm and as feedback to the arm planning nodes [9].

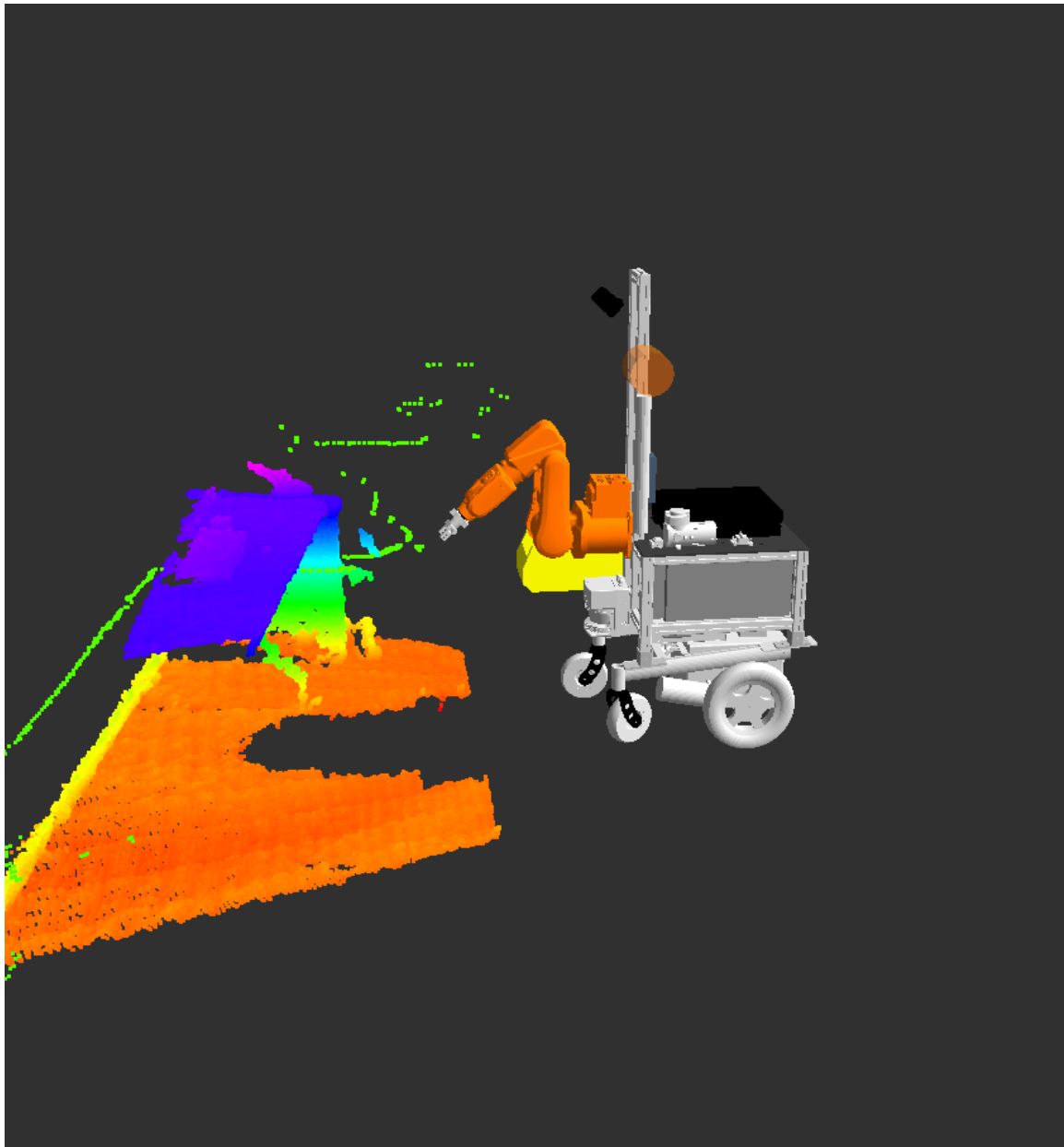


Figure 3.10: ABBYs robot model, LIDAR data (green points), and Kinect point cloud (multicolored points) visualized in Rviz

Chapter 4

Experimental Software

New software packages were developed and integrated with existing open source packages for ABBY. Some of these packages increase the capabilities of the platform, and others were used to test those capabilities. These include navigation and planning, calibration procedures, and investigations into industrial applications.

4.1 Mobile Base Planning

ABBY's mobile base is controlled by software that performs localization, which determines where the robot is in its environment, high level path planning, which determines a feasible course from the current location to the desired location, and trajectory planning, which determines a sequence of velocities for the robot to execute in order to arrive at the desired location.

ABBY performs localization by fusing odometry and Adaptive Monte Carlo localization methods to create a reliable, accurate estimate of the robot's position. Two standard ROS mobile base planners develop global and local plans to specified waypoints.

4.1.1 Localization

In robotics, localization is the task of determining where the robot is. Localization methods can be classified into one of two groups. Relative localization methods determine the robot’s location with respect to the robot’s previous location, and absolute localization methods determine the robot’s location with respect to an absolute reference in the robot’s environment, sometimes called the “ground truth.” There are advantages and disadvantages to both classes of localization methods, and ABBY’s localization uses a combination of relative and absolute localization to mitigate the disadvantages and leverage the advantages of each.

A benefit of relative localization methods is that they are computationally simple. Odometry on ABBY uses fourteen mathematical operations (seven addition, four multiplication, and three trigonometric, as shown in Algorithm 1.). This allows for high frequency update rates and implementation on embedded processors or in logic circuitry.

Algorithm 1 Odometry update from differential wheel encoder measurements. d_r and d_l are the difference in encoder counts since the last update. trans is the translation. d_x and d_y are the translation in the x and y directions. d_θ is the rotation in θ , and θ is the heading.

```
 $d_r \leftarrow r - r_0$ 
 $d_l \leftarrow l - l_0$ 
 $\text{trans} \leftarrow k_t * (d_i + d_r)$ 
 $d_x \leftarrow \text{trans} * \cos(\theta)$ 
 $d_y \leftarrow \text{trans} * \sin(\theta)$ 
 $y \leftarrow y_0 * d_y$ 
 $d_\theta \leftarrow \arcsin(k_\theta * (d_r - d_l))$ 
 $\theta \leftarrow \theta_0 + d_\theta$ 
```

Further, relative localization requires no knowledge of the robot’s environment (such as a map), and it does not require the robot’s environment to be instrumented with sensors to track the robot or beacons for the robot to track. Relative localization can also be accomplished with relatively cheap sensors such as inertial measurement

units (IMUs), optical flow sensors, and (in the case of wheeled vehicles) shaft encoders.

However, relative localization methods all accumulate error over time. Each update is performed with respect to the previous, and the superposition of successive errors causes the cumulative error to increase. The source of the error may be physical, such as wheel slip, or computational, such as the non-linearity of the trigonometric function used to estimate the heading in Algorithm 1. A well-calibrated relative localization system with an accurate observer model will still accumulate error over time, and the estimated position of the robot will slowly diverge from the true position. This was demonstrated using ABBY’s odometry system; see Section 4.1.1.

Unlike relative localization, absolute localization does not accumulate error. There are several different types of absolute localization methods that use different types of sensors. Some methods use external sensors, such as cameras or radio frequency (RF) tracking systems to monitor the robot’s position. In order for a robot to use these methods, the operating environment must have already been instrumented with the necessary sensors. Other methods use sensors on the robot to track features of the robot’s environment and compare them to a known map of the robot’s environment [21]. Trackable features may already exist in the environment, such as ceiling lights in an office building, or may be added, such as position-coded labels on a warehouse floor. Systems with ranging sensors can track features of the geometry of the environment itself. To perform an update, all of these localization methods compare sensor data to a map or model of the environment to estimate the robot’s position. This means that they are dependent on an accurate map or model, which may not be possible in an environment with changing features. Methods using sensors onboard the robot also depend on the environment having suitable features to localize against, which may not be true in environments such as open fields or environments with many repeated similar or identical features such as long hallways.

Although most absolute localization methods require an *a priori* map (or model)

of the environment, one class of absolute localization methods performs simultaneous localization and mapping (SLAM). SLAM algorithms begin with no map of the robot’s environment and incrementally build one as they explore. A SLAM algorithm using a LIDAR can exploit partially-overlapping LIDAR scans to register new scans with respect to previous scans. The translation and rotation required to register the scan can be used to determine the robot’s position with respect to the previous position. Each new scan increases the known region of the environment, slowly building a map [21].

ABBY’s sensor suite contains several sensors that can be used for localization. The encoders on the wheels are well-suited for odometry. The LIDAR and the Kinect depth camera can both be used for absolute localization using a number of methods, including both SLAM and *a priori* map localization algorithms. In addition, the Kinect camera could be used for localization based on patterns on the floor. Of these possible methods, odometry was chosen for relative localization, and Adaptive Monte Carlo Localization (AMCL) using LIDAR scans and an *a priori* 2D occupancy grid map was chosen for absolute localization.

ABBY uses odometry from the encoders on the wheels for relative localization. The physical state observer runs under the real time operating system on the cRIO, and publishes pose estimates with uncertainty (represented as covariance) to the ROS system at 50 Hz. Relatively high frequency updates to the robot’s pose are required as an input to the local planner, which generates velocity pairs at a rate of 12 Hz.

A SLAM algorithm was considered for absolute localization on ABBY. Because SLAM does not require an *a priori* map, it would be easy to install a SLAMing robot in a novel environment. Maps were generated by ABBY using the LIDAR and the gmapping SLAM package [22]. Gmapping uses a Rao-Blackwellized particle filter to generate maps as it localizes. Gmapping on ABBY was unable to reliably traverse doorways without introducing error. This was sufficient reason not to use it

for localization.

Instead, the maps were manually cleaned up using image editing software and used as *a priori* maps for AMCL. AMCL is an absolute localization method that models the robot’s pose as a probability distribution [21]. The robot’s pose is considered probabilistic to represent the uncertainty of the sensor measurements used to determine the pose. ABBY uses AMCL to match LIDAR scans to an *a priori* map. AMCL can theoretically solve the “wake-up robot problem,” in which the robot is initialized with no estimated pose. However, testing with ABBY showed that AMCL could not reliably solve this problem, and would often converge on a false pose estimate. Instead, ABBY is initialized to a pose at or near the true pose, with sufficiently large covariance that the true pose is within the likely region of the estimated pose. As the robot runs, the pose estimate will converge on the true pose. On ABBY, each pose update from AMCL takes approximately 200 milliseconds, so it can run no faster than 5 Hz.

Combining odometry with AMCL yields results that are better than either one alone. Because AMCL takes so long to compute, it cannot be used to approximate continuous localization. The local planner for the mobile base updates at 12 Hz, which is faster than AMCL can update. Whereas odometry is more suitable for the local planner, the error it accumulates as the robot runs eventually makes it unsuitable for global planning.

The results of two methods are fused by storing two transforms in the robot’s TF tree, as shown in Figure 4.1. One transform is between the robot’s base_link (a coordinate frame with its origin on the floor between the robot’s wheels) to its parent, the odometric frame odom. This transform is updated by the odometric state estimator on the cRIO at 50 Hz and provides a higher resolution position estimate. Local planning is performed in the odom frame. The top level transform is from the map frame (the absolute coordinate system) to the odom frame. This transform is updated by

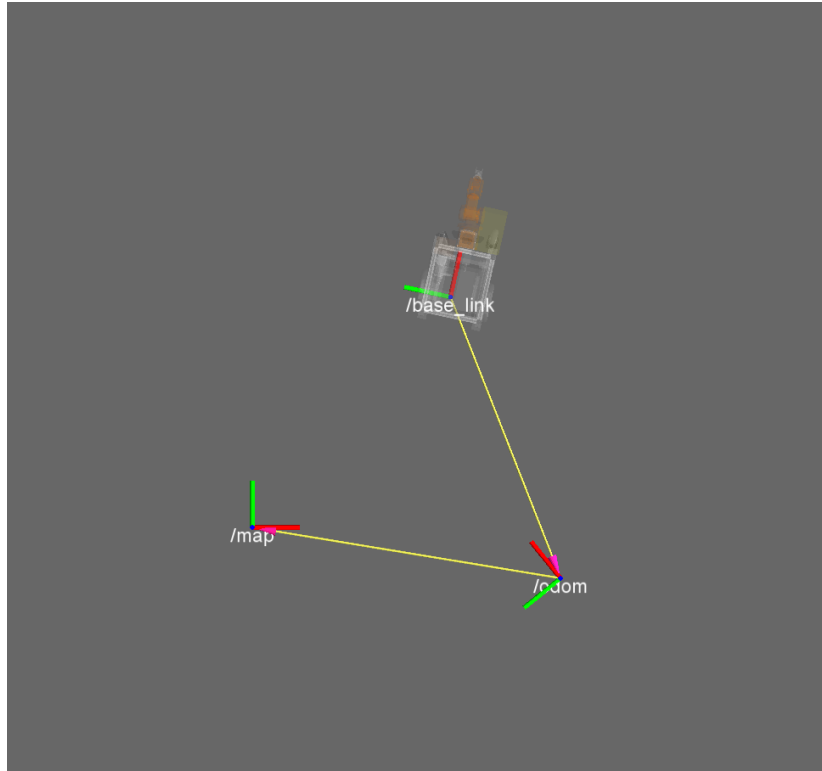


Figure 4.1: The map, odometry, and base frames of the robot localization system.

The transform from the world frame map to the odometry frame, generated by AMCL, cancels out the accumulated error in the transform from the odometry frame to the robot's base frame, generated by odometry.

AMCL, which runs an update every time the robot moves more than 0.05 meters in translation or 0.1 radians in rotation. On each AMCL update, the transform from the map to odom frame changes such that it cancels out any error in the transform from the odom frame to the robot's base_link. Over a long period of operation, the odom transform may accumulate significant error, but the transform from the map frame to the base_link remains accurate because of the absolute localization updates.

4.1.2 Mobile Base Trajectory Planning

One of the major tasks for a mobile robot is navigation through its environment. In an industrial application, the location may be retrieved from an inventory database, or it may be specified by a human operator, but the robot's task is the same. From its

current location, the robot must plan a path to another location in its environment. The path must avoid obstacles, and it should be as direct and efficient as possible. The robot must then generate a trajectory to follow the path and travel to the goal location. The trajectory cannot violate the dynamic constraints of the robot. Given a trajectory, the robot must execute it by controlling the actuators as accurately as possible to adhere to the desired path and trajectory.

Speed control on ABBY was implemented by previous researchers as a pair of PID controllers, one for each wheel. The PID controllers are implemented on the cRIO's FPGA for speed and robustness, with loop closure rates of 100 Hz. A simple geometric algorithm (see Equations 1 and 2), implemented on the cRIO's PowerPC processor, is used to convert twist-style commands (forward and rotational speed) into speed setpoints for each wheel. Each PID controller's setpoint is specified in meters/second and its output is an 8-bit signed integer. These signed integers represent the desired voltage to be output by the Sabertooth motor controller, with -127 being full reverse and 127 being full forward. Since the Sabertooth motor controller can vary its voltage output from -24 volts to 24 volts, the 7 bits of speed resolution in each direction correspond to a voltage output resolution of about 189mV. The PID controllers on ABBY were originally tuned for another robot with the same mobility platform but a different weight distribution [23]. With some retuning, ABBY's minimum achievable forward/reverse speed is 0.1 m/s and minimum rotational speed is 0.35 rad/sec; other robots based on the same mobility platform were able to achieve 0.1 m/second and 0.1 radians/second respectively.

$$v_{left} = v_x - \frac{w_{track}}{2} * v_{yaw} \quad (4.1)$$

$$v_{right} = v_x + \frac{w_{track}}{2} * v_{yaw} \quad (4.2)$$

The higher-level components of navigation are path and trajectory planning. Path planning is the task of determining a path from the robot’s current location to a desired pose. Trajectory planning takes the path and determines a series of velocity commands to move the robot through the path without violating the acceleration and velocity constraints of the robot. On ABBY, these tasks are performed by a global and a local planner, respectively.

NavFn [24], the global planner node available in the ROS navigation stack, operates on a grid-based global costmap populated by data from the LIDAR. Given a desired pose, NavFn finds a minimum-cost path using Dijkstra’s algorithm [25]. This path is defined as a series of intermediate robot poses along the path. NavFn successfully plans paths for ABBY in relatively open environments, but because it assumes a circular robot base, it will sometimes plan impossible paths in crowded environments.

The local planner generates trajectories to follow the path produced by the global planner; it operates on a local costmap populated by data from the LIDAR. The robot performs local planning using a trajectory rollout approach [21], which forward-simulates translational and rotational velocities and evaluates the resulting trajectories for proximity to obstacles, proximity to the goal, and adherence to the global path. These scores are weighted and summed to determine the velocity command’s score. The highest scoring velocity command is sent to the mobile base driver

4.2 Inverse Kinematics Solver

An important part of robotic arm planning is an inverse kinematics solver. Given a pose in the robotic arm’s work envelope, an inverse kinematics solver determines a set of joint angles that would place the end effector at that pose. Because not all poses have possible solutions and some poses are degenerate cases, analytical inverse

kinematics solvers are mathematically complex.

ROS includes a kinematic solver in the kinematics_constraint_aware package that wraps the inverse kinematics solver of the Orocosp project’s Kinematics and Dynamics Library (KDL) [26] [27]. The KDL solver is a numerical solver that uses Newton-Raphson iterations. The KDL solver takes joint angle limits into account in evaluation of its solutions, only returning a solution with valid joint angles. However, the KDL solver will often fail for achievable poses and, because it uses an iterative numerical method, runs slowly, on the order of tens of milliseconds.

To counteract the problem of the KDL solver failing for achievable positions, the solver was wrapped in a method to retry the search on failure. When the solver fails to find an inverse kinematics solution for a desired pose, the solver is reseeded with randomly selected joint values and called again, up to 100 times. To test the solver, poses were generated using forward kinematics of simulated joint angles. Since the poses were generated by forward kinematics, they are guaranteed to be achievable. Many of the test poses were not solvable by the unmodified kinematic solver, which only made one attempt at a solution. When the number of attempts was increased to 100, the success rate was 32% for solvable poses.

As shown in Figure 4.2, most inverse kinematics requests are solved in under 20 iterations or will fail. Since the seed is random, the number of requests needed to solve for a difficult pose is probabilistic, and though some positions are more difficult to solve for using KDL’s iterative approach, there is no guarantee that the solver will succeed or fail for a given pose. The resulting inverse kinematics solver is suitably reliable, though slow, taking as long as 3.5 seconds before determining that a pose is unsolvable. This is acceptable for the robot at this time, but a faster, more reliable inverse kinematics solver will be necessary in an industrial installation.

The OpenRAVE project includes the IKFast kinematic solver tool [27], which analyzes a kinematic chain and generates C++ code for an inverse kinematics solver

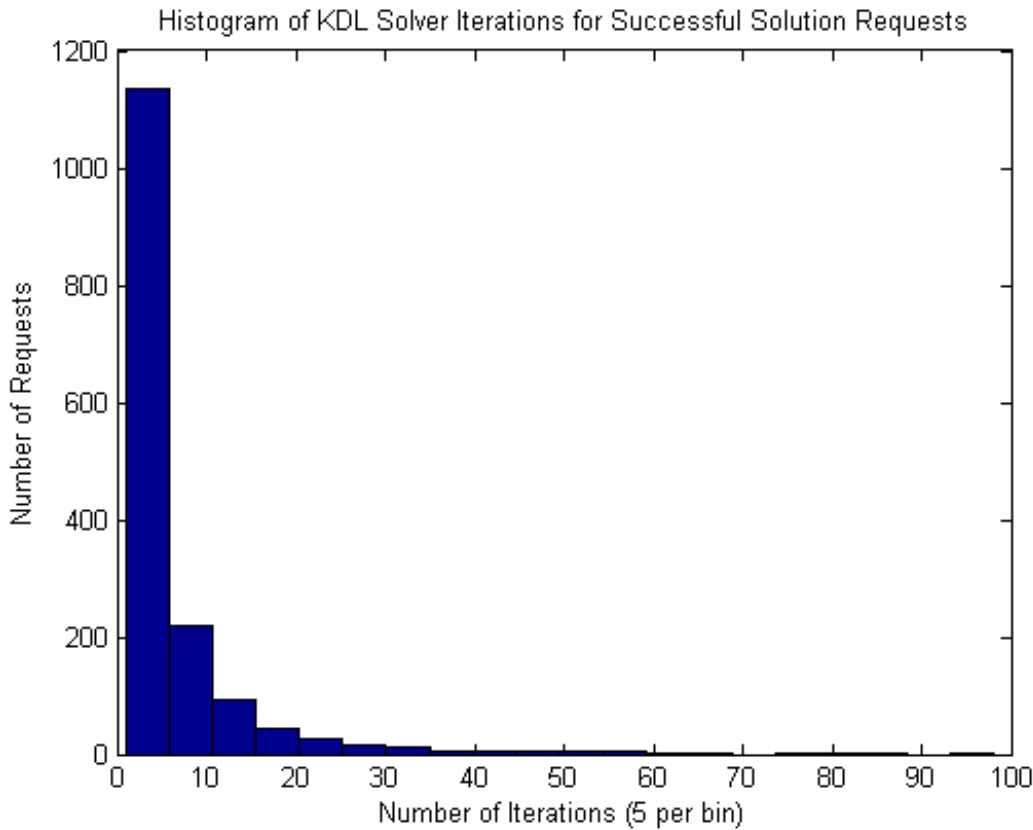


Figure 4.2: A histogram of the number of iterations required for the KDL inverse kinematics solver to solve for achievable pose requests.

5000 poses were requested, of which 1583 were solved in less than 100 iterations.

for that chain. The solver it generates is a closed-form analytic solver, meaning it runs very quickly (<1 ms) and can handle the vast majority of achievable poses, including degenerate cases. The greatest limitation of IKFast is that it does not take into account joint limits, but assumes that all joints can rotate freely. This means that IKFast will often generate solutions that are unachievable for a rotation-limited robotic arm.

The ROS wrapper for IKFast rejects solutions that violate joint constraints, but IKFast will only return the first eight IK solutions it finds, and it is likely that none of these solutions will satisfy joint constraints, particularly for degenerate cases. When this happens, the ROS inverse kinematics service fails, despite the possible existence

of a valid solution. It may be possible to rewrite the IKFast compiler or modify the generated code to work with joint limits, but at this time, IKFast was determined to be unsuitable for arms of ABBY’s geometry due to the high incidence of solver failure.

4.3 Arm Navigation

ABBY’s arm navigation package is closely based on the standard ROS arm navigation package, which is generated from a URDF by a tool called the Planning Description Configuration Wizard. This wizard allows the user to define a manipulator kinematic chain from a URDF file and then generates an arm navigation application, including the necessary launch files for an inverse kinematics plugin, a planner, and a collision environment server. This ”default” arm navigation application was augmented with filtering nodes for the Kinect data going into the collision environment and the modified KDL inverse kinematics plugin described above.

The trajectory planner for the arm is the default planner available with the ROS arm navigation package. It uses a sample-based planning algorithm from the Open Motion Planning Library called Single-Query Bi-Directional Probabilistic Roadmap Planner with Lazy Collision Checking (SBL) [28]. SBL plans collision-free paths for the arm and publishes these paths as ROS trajectory messages, which the ROS Industrial arm driver executes. Because SBL performs all of its planning in joint-space, the arm navigation application uses the inverse kinematics plugin described above to convert goal poses into joint space before planning paths to them.

4.3.1 Collision Detection

The robot uses the ROS node Collider to maintain a collision map, a 3D occupancy grid represented by an Octomap oct-tree. The collision map is populated by data from

filtered Kinect point clouds. In addition to this "raw" map, a collision environment is maintained, which contains information from this map and keeps track of detected objects such as the manipulable objects detected by the tabletop box recognition system described below. The objects are given IDs and stored in the map as meshes or geometric solids, enabling the arm navigation code to make decisions about whether collisions are allowable.

The arm navigation code navigates around obstacles in the collision environment, including the robot itself, preventing the robot from damaging itself and the objects around it. Collisions can be selectively allowed between robot links and objects in the collision environment. For instance, it is impossible to pick up an object without the jaws of the gripper colliding with it. When creating a request to make the final approach to pick up an object, collision detection between the gripper jaws and the object is disabled, allowing the robot to pick the object up while still preventing collisions between the robot and other obstacles.

4.3.2 Kinect Data Filtering

The Kinect's field of view includes the robot's arm, which the collision detection process would classify as obstacles. This causes the robot to freeze because it is in collision with a perceived obstacle, even though the obstacle is the robot itself. In order to prevent this, the Kinect point cloud is pre-filtered to remove points that are within the robot volume, which is determined by padding the 3D model of the robot generated from the URDF. The resulting point cloud, which has all points within the robot removed, is used for all collision monitoring and object detection. This is a computationally intensive task, consuming one full core of the PC's processor.

4.4 Tabletop Box Manipulation

Once ABBY arrives at the desired location in the factory, it must identify objects and pick them up from the inventory shelves. This is an area of future research, but a basic object perception and manipulation system was implemented as a proof of concept. The system uses several object detection nodes developed by Willow Garage for the PR2 robot, as well as two nodes written specifically for this project.

The Object Manipulation Controller was written specifically for this project and serves as the central control node, translating and routing messages between the perception and manipulation nodes. It provides a callable method `pick_objects()`, which performs the task described in Algorithm 2.

Algorithm 2 The process for detecting, picking up, and stowing the objects on a table.

```
detected_objects ← tabletop_detection(kinect_data)
for all object in detected_objects do
    if graspable(object) then
        pick(object)
        place(object)
        stow_arm
    end if
end for
```

The `tabletop_detection()` step is performed by the `tabletop_object_segmentation` package, developed by Willow Garage [29] for the PR2 robot. This software identifies a tabletop surface in a point cloud from the Kinect using RANSAC [30] and adds it to the collision environment as an object. Objects on top of the table (`detected_objects`) are segmented into separate point clouds and inserted into the collision environment as Graspable Objects. These Graspable Objects are used later by the manipulation package during the `pick()` step to identify and locate the objects in the robot's environment. The `pick()` and `place()` steps are performed by the box manipulator node, which exposes them as action services using a standard pick-and-place API defined in ROS. This standard API allows the box manipulation package to be easily replaced

by a new manipulation package or the manipulation controller to be replaced by a more sophisticated package. In the final step, `stow_arm()`, the arm is moved to a predefined stowed position, which minimizes the robot's footprint while it is driving.

4.4.1 Box Manipulation

The box manipulator node was written for this project to lift small objects from a shelf or table and place them. It provides two services—one to pick up a graspable object, and one to place the currently held graspable object at a set of coordinates.

When the manipulation controller calls the pick service on a Graspable Object in `detected_objects`, it uses another node created by Willow Garage for the PR2 to fit a bounding box to the Graspable Object's point cloud. Though the objects being manipulated are cylinders, a bounding box is a fairly accurate representation of the object. This bounding box is then used to generate an approach path composed of two poses. The first is a pregrasp pose close to the object, with the gripper pointed at the object center and the gripper jaws parallel to the sides of the bounding box. This pose is sent to the arm navigation package, which generates a trajectory and moves the arm to the pose. The second pose is the grasp pose, with the object between the gripper jaws. This pose is also sent to the arm navigation package, and once the robot is in the grasp pose, the gripper is closed around the object.

Once the gripper is closed around the object, the object manipulation controller calls the place service with a pose above the robot's onboard storage bin as a target. This service sends the pose to the arm navigation package, which generates a trajectory and moves the arm to the bin. The gripper is then opened, dropping the object in the bin.

4.5 Calibration

In order for the point cloud data from the Kinect to be usable for arm navigation, the positions of the Kinect and the arm must be correctly registered in 3D space. Because the position of the Kinect camera’s optical frames within its housing are not precisely known, it was necessary to perform a simple extrinsic calibration routine to determine the position and yaw angle of this frame.

To determine the height (z-axis position) and pitch angle of the Kinect, the robot was placed so the Kinect had an unobstructed view of the floor in front of it. RANSAC [30] was used to fit a plane to the floor, and the transform from the fitted plane to the Kinect was calculated. A similar method was used to determine the x-axis position of the Kinect. The robot was placed so that the Kinect had an unobstructed view of a wall at a known distance in front of it, and RANSAC was used to fit a plane to the wall. The distance of the wall plane was then used to calculate the x-axis position of the Kinect. The y-axis position of the camera was estimated to be centered on the robot, and the y-positions of the lenses were determined from the CAD model of the Kinect.

With the position of the Kinect now known, it was necessary to precisely determine the pose of the arm relative to the Kinect. Due to the length of the arm, a small error in the orientation of the arm could cause significant disparity between coordinates in the Kinect’s frame of reference and the position of the robot’s gripper calculated using forward kinematics. The pose of the arm base was originally taken from the CAD models used to design the robot, but the model’s fidelity to the robot was not sufficiently precise.

A more precise transform was calculated from test data using Mathematica. Given a set of data points, the program calculates the transform (translation and rotation) between the Kinect and the arm base link that minimizes RMS error in the position of the gripper tip. Each data point consists of the position of the tip of the gripper

with respect to the Kinect, measured from a manually-selected point in the Kinect point cloud, and the pose (position and orientation) of the gripper with respect to the base link of the arm, calculated by ROS’s TF server using forward kinematics. This program was run using an input dataset of twenty-five points, and the resulting transform was used in the robot’s URDF to define the position of the arm with respect to the Kinect.

4.6 QR Code Recognition and 3D Localization

Mobile manipulators in industrial settings can benefit from information about the objects they manipulate. Most of the explorations of object manipulation have been directed toward general purpose object recognition and manipulation, but the problem of determining how to pick up an object can be greatly simplified by simply putting manipulation information on the object itself. For more complex information, the object could link back to an entry in a database. Properties salient to mobile industrial manipulation, such as grasp affordances, mass, volumetric data, and visual cues for registration and localization, can all be encoded into visual or RFID tags on manipulable objects. To this end, an exploration was made into using the Kinect in conjunction with a higher-resolution camera to read QR code tags on boxes and use the QR code to perform 3D localization of the box.

QR codes can hold up to 3 kilobytes of data, or 174 bytes with 7% error correction. They include 3 ”finder square” fiducials, which can be used to acquire and correct the skew and size of the code. QR codes are already used throughout the automotive industry for part labeling [31].

Information about how to grip an object can be stored in a small amount of data in a QR code on an object. This information, the “affordance cue,” contains, in a compact form, information that aids a robot in deciding how to manipulate an object:

1. If an object has handles, the affordance cue contains the information necessary to define the handles and locate them relative to the tag.
2. If an object can be lifted only from the bottom, as with a fork-lift, the affordance cue contains information necessary to locate the bottom of the object relative to the tag.
3. If the object can be grabbed from the sides by a gripper, the affordance cue contains gripping force constraints and the information necessary to locate the sides relative to the tag.

Using a Kinect sensor and MatLab, a rudimentary proof-of-concept was tested for boxes with handles on top. Because the Kinect image sensor does not have high enough resolution to read QR codes, it must be supplemented with a second, higher resolution camera extrinsically calibrated to the Kinect. This part of the detection was simulated, and the QR code data manually entered into the program. The coordinates of the three finder points in the Kinect RGBD image are then used to get the positions of the three finder points in 3D space. Again, because a high resolution camera was not available, this step was simulated by manually picking points. Using the 3D coordinates of the 3 finder points, it is possible to localize the QR code in 3D space, including both position and orientation. Using the location of the tag and the tag's information about the handle's location relative to the tag, the handle can be located, allowing a robot to grasp it without knowing any other information about the box. The results are shown in Figure 4.5.

Because the Kinect RGB camera does not have sufficiently high resolution for the task, these experiments were not performed on the robot. However, this line of research is one of the planned future purposes of the robot, once a high resolution camera can be acquired, mounted, and calibrated to the Kinect.

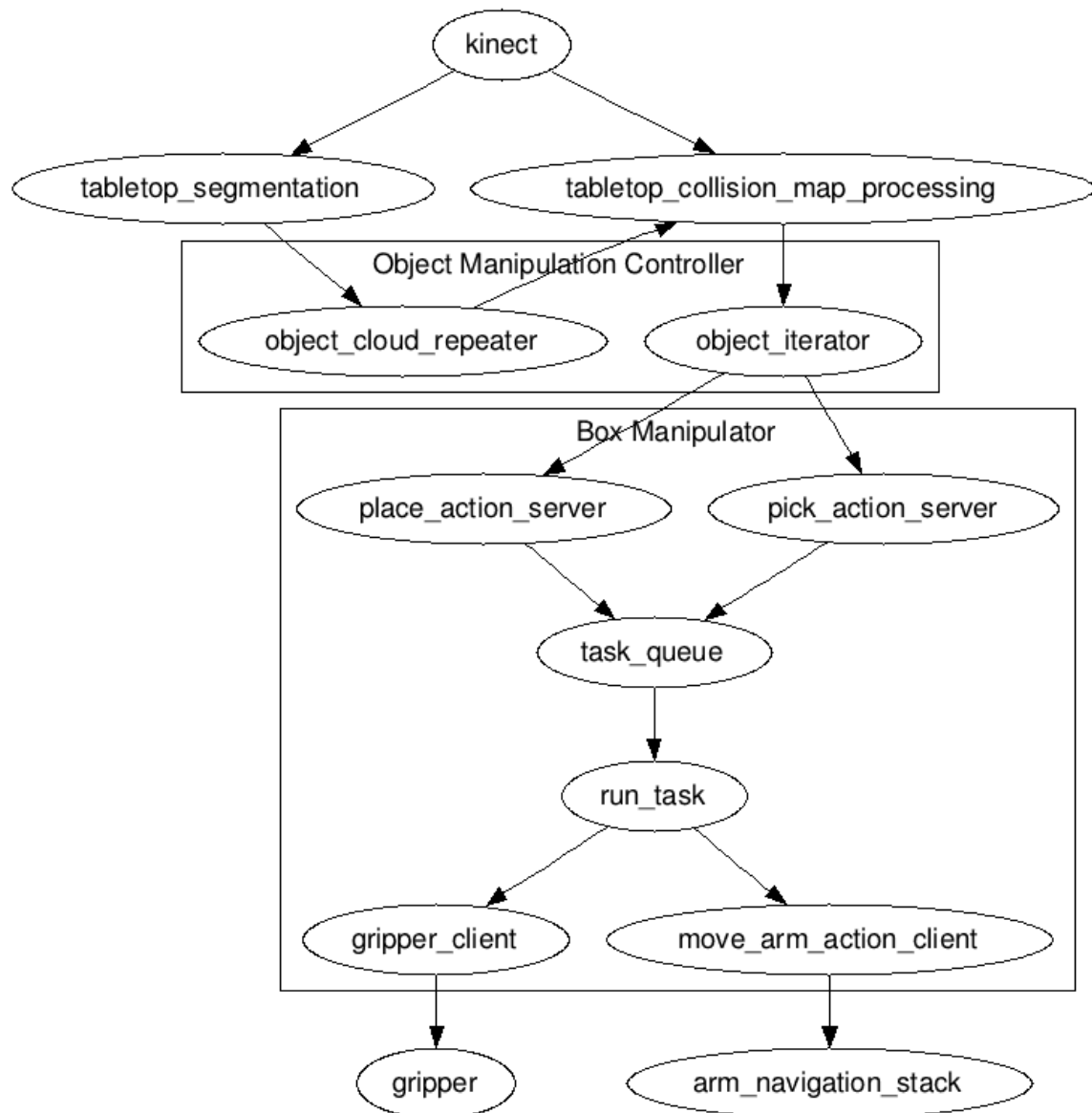


Figure 4.3: The box manipulation pipeline

Data from the Kinect is used to locate boxes on a table, which are then picked up and placed in the bin.



Figure 4.4: QR Level 3 code

(Source: Wikipedia, licensed under Creative Commons Attribution Share-Alike License)



Figure 4.5: A box localized using the QR code.

Red dots are the QR code finder pattern. Blue is the projected handle center. Green are the handle corners.

Chapter 5

Industrial Safety

Mobile robots, particularly experimental platforms, require safety systems to disable them. These systems fall into two major categories. Reflexive collision avoidance systems keep robots from colliding with humans interacting with the robot. Emergency stop systems are used to disable the robot in case it does something unsafe or unexpected. Both types of systems are necessary in an industrial robot, especially one that does not operate in a cage or with guards, neither of which are practical for a mobile robot.

5.1 Reflexive Collision Avoidance

A key safety feature of many robots is reflexive speed limiting or halting. Reflexive collision avoidance uses sensors to detect obstacles in the robot's path and prevent motion that would result in a collision. Reflexive collision avoidance is particularly important for robots that operate in shared environments with people, because people can suddenly move into a previously clear robot path, endangering themselves and the robot. Whereas a planner will create safe paths for a robot around static obstacles, paths may be invalidated by moving obstacles such as people, and the planner may react too slowly to prevent a collision. Reflexive collision avoidance operates more

quickly and on a lower level than planning and trajectory generation, and can override the velocity commands from the trajectory generator.

At this time, ABBY does not implement reflexive collision avoidance for the base or the manipulator. Because both operate at low speeds, the robot does not pose a safety threat to the operator and can be easily stopped with the emergency stop system described below. Before the robot can be tested or deployed in an industrial environment, and to allow for faster movement, reflexive collision avoidance must be added. Proposed methods for reflexive collision avoidance are described in Appendix 3.

5.2 Emergency Stop System

5.2.1 E-Stop Systems Used in This Lab

The Case Mobile Robotics Group has used a few emergency stop systems in its robots. All of the HARLIE-class robots developed for the Intelligent Ground Vehicle Competition used a commercially-available wireless relay system from Remote Control Technologies. This system consisted of the remote control relay in series with an onboard disable switch and a second relay switched by an active-high enable signal from the cRIO, which is software-controllable. These three switches (one manual and two relay) control the current through the coil of a solenoid, which in turn switches the power to the motor controller on and off. This system has one critical flaw, which is that there is no “heartbeat” from the wireless remote to the remote control relay. This means that if the battery in the wireless remote dies or the radio communication is lost between the wireless remote and the robot, there is no way to remotely stop the robot, nor is there any indicator to the operator that the robot cannot be wirelessly stopped.

OTTO the smart wheelchair could operate in either autonomous or manual control

modes, and used a custom remote system to enable and disable autonomous mode. Using the GPIO mirroring function of a pair of XBee 2 Pro wireless network modules, a digital signal was transmitted from a remote control unit to the input of the Arduino controlling the wheelchair's motor controllers, disabling the autonomous functions of the wheelchair when a button was pushed on the remote. Because the XBee wireless modules' GPIO mirroring has a programmable timeout and default output state, this system automatically disabled autonomous functions if communication was lost between the remote and the robot. However, this system relied on an Arduino microcontroller and was not designed as an emergency stop system, but as a switch between autonomous operation and normal (joystick) operation of a wheelchair.

5.2.2 E-Stop Requirements

This robot has several requirements that motivated the development of a new emergency stop system combining the merits of the HARLIE-class stop system and the OTTO remote switching system. First, the emergency stop system needs to be able to switch the high current, 24 volt rail providing power to the motor controllers. Second, the system needs to be able to activate the 24 volt emergency stop input on the IRC5 robot controller, which must be electrically isolated from the rest of the robot's DC electronics. Third, the system must monitor four sources, stopping the actuators if any of them are disabled:

- 5 volt active-high enable signal from the cRIO, which is controlled by the ROS software
- 24 volt active-high emergency stop signal from the IRC5, which is controlled by the emergency stop switches on the IRC5 and FlexPendant and by RAPID software.
- Twist-lock stop switch mounted on the robot (The robot is disabled if the switch

is opened or disconnected.)

- Wireless remote control with a heartbeat signal of at least 1Hz

Fourth, the system should be implemented entirely in hardware for safety reasons. Software faults in a safety system are unacceptable and adequate testing of a software system would be too time-consuming for this project. Fifth, the remote control unit should have some feedback as to the state of the four emergency stop sources described above.

Given the requirements, an emergency stop system was designed and fabricated using printed circuit boards. The schematic of the system is shown in Figure 5.1 and Figure 5.2. The system consists of two circuits, a remote control and an emergency stop circuit on the robot.

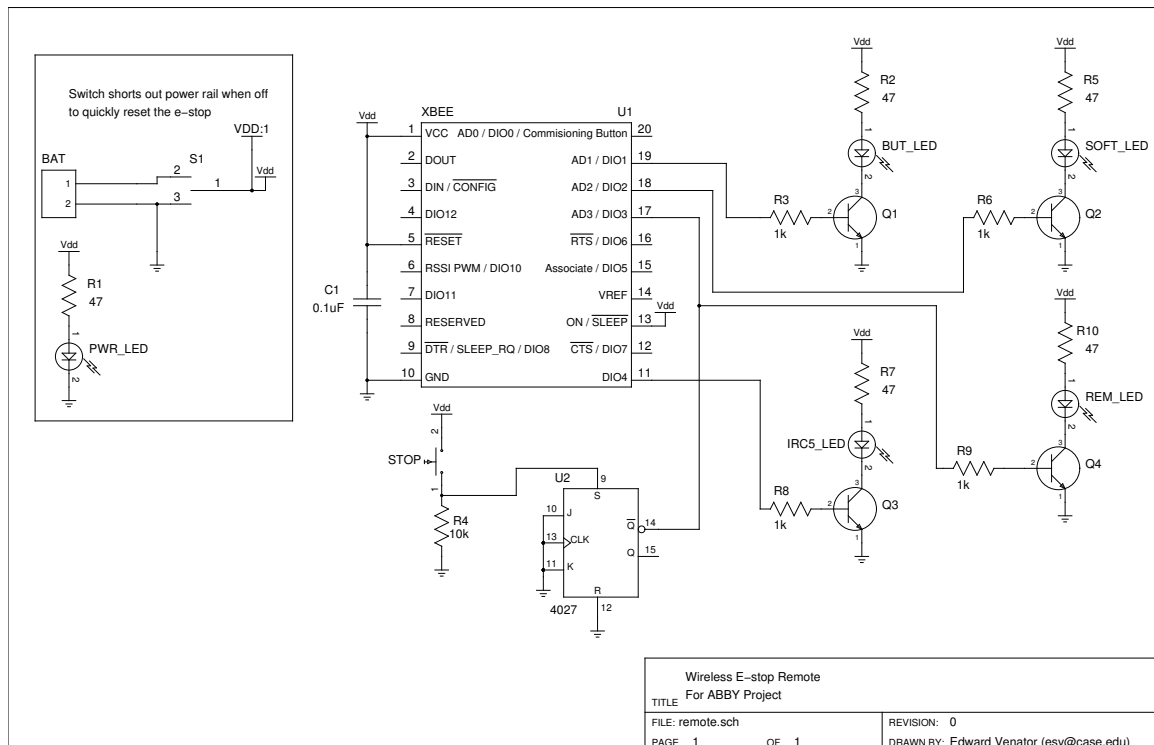


Figure 5.1: Schematic of the emergency stop remote tested on ABBY.

The remote uses an XBee radio to send an enable signal to the robot and receive the current emergency stop status from the robot, which is displayed with LEDs.

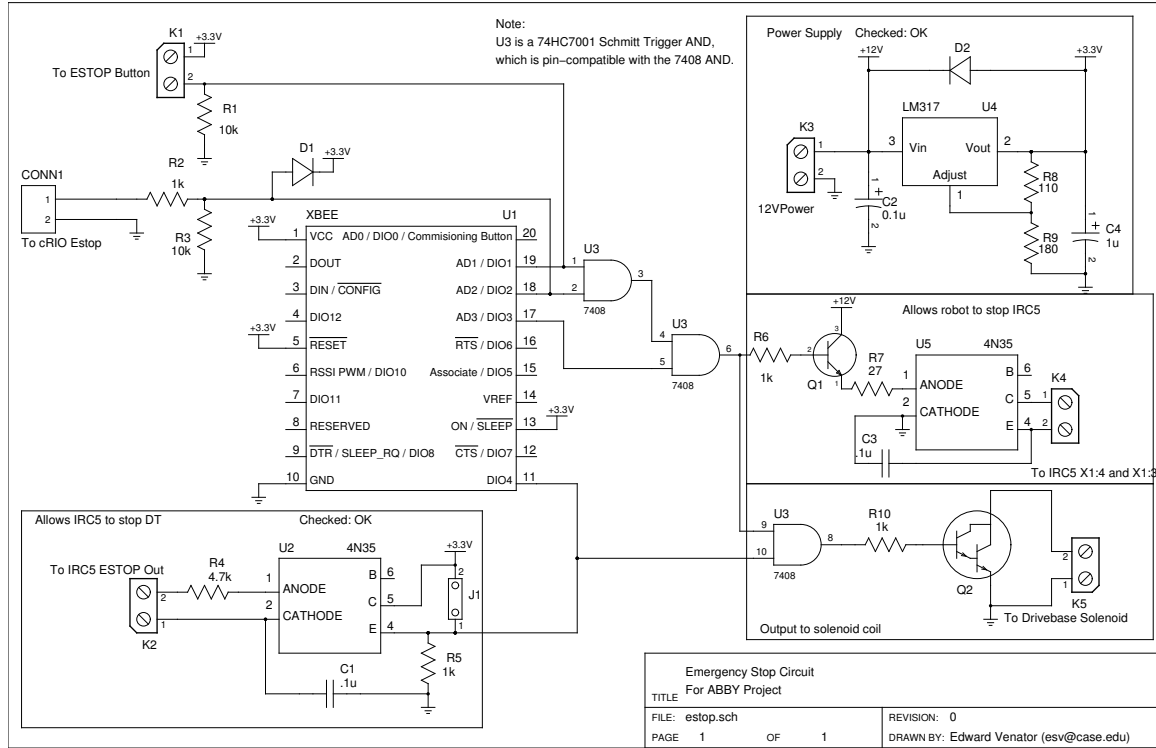


Figure 5.2: Schematic of the emergency stop receiver and aggregator on ABBY

The remote circuit uses an XBee radio module's GPIO mirroring function to transmit the state of the emergency stop button to the emergency stop circuit on the robot in the same manner it was used on OTTO. This system also uses the GPIO mirroring function to send the states of the onboard emergency stop sources to the remote, where they are displayed on LEDs. Because a twist-lock style emergency stop button was not available, an S-R latch was used to latch the state of a normally-open momentary pushbutton, requiring that the remote be powered off and back on again to reset the wireless emergency stop. If communication between the XBEE modems is interrupted for any reason, DIO3 in the emergency stop circuit goes low, disabling the robot.

The emergency stop circuit on the robot has inputs for the onboard emergency stop button, the cRIO's enable signal, and the emergency stop output of the IRC5. The input from the IRC5 goes into an optoisolator IC because the I/O on the IRC5 is floating relative to the rest of the robot's DC systems. A 7400 series AND IC is

used to generate logic signals to enable the drive base and the IRC5's emergency stop input. The drive base logic signal controls a Darlington transistor, which in turn switches the coil of a solenoid that controls the drive base in the same manner as on HARLIE-class robots (not shown in Figure 5.2; see Figure 3.4). The IRC5 output logic signal switches the 24v General Stop input of the IRC5 using an optoisolator IC.

These circuits were prototyped and installed on the robot. Because the RAPID software running on the IRC5 was not configured to output the emergency stop state, the input from the IRC5's emergency stop was defeated by installing jumper J1. Additionally, testing showed that the 4N35 optoisolator used to switch the IRC5's emergency stop could not sink enough current to enable the emergency stop circuit, causing the IRC5 to go into General Stop mode seemingly at random. The ability to control the IRC5's emergency stop state was defeated by disconnecting the IRC5 Stop output and shorting the General Stop input on the IRC5. These two changes completely decouple this emergency stop circuit from the IRC5. Furthermore, the wireless link between the XBee modules proved unreliable, causing the system to momentarily switch into emergency stop mode seemingly at random. Extensive bench testing of the system suggests that this problem is caused by an insufficiently reliable power supply to one or both of the XBee modules. In order to make the system usable, the wireless emergency stop was replaced with a twist-lock style emergency stop button on a ten foot wired tether. The system does reliably control the power to the drive base, providing a level of safety for the robot, but revisions are required to gain the full functionality of the original design.

A revised version of this emergency stop system is described in Appendix 2. The revised version has been designed, and all of its subsystems have been tested, but it has not yet been implemented on the robot. The revised emergency stop system includes a wireless remote and full integration with the IRC5's emergency stop systems.

Chapter 6

Validation Results

6.1 Localization

ABBY’s odometry system was evaluated by performing two tests without the benefit of an absolute localization system. These tests serve to characterize the error accumulation in the odometry, and the results motivated the use of absolute localization on the robot.

In the first test, the robot was manually driven in a straight line for ten meters in the positive x direction. The start and end points were marked on the floor, and the robot was teleoperated in a straight line between them. At the end of each trial, the robot’s estimated position, as measured by the odometry system, was recorded. The results of these tests are in Table 6.1; no wheel slip was observed during any of these trials. Perfect localization would have observed the robot to be at $x = 10.0$ meters and $y = 0.0$ meters. The results, as expected, show relatively accurate absolute displacement, but relatively large errors in the position estimate (up to 2.908 meters) due to errors in the heading estimate. Some of the error was introduced by the robot being visually aligned to the start and stop marks on the floor, but some is the result of wheel slip and linearization error in the odometry.

Table 6.1: Ten meter odometry test

Trial	X	Y	Displacement	Position Error
1	9.535	-2.908	9.969	2.945
2	10.042	-0.760	10.071	0.761
3	10.373	-0.032	10.373	0.374
4	9.996	-0.454	10.005	0.454
5	9.881	-0.663	9.903	0.674
6	10.019	-0.610	10.036	0.610
RMS	9.977	1.294	10.060	1.318
STD	0.271	1.016	0.164	0.978

Measurements in meters

In the second test, the robot was manually driven for five laps of a circle with a 1 meter radius. The start and end points, as well as the circle for the robot to follow, were marked on the floor, and the robot was teleoperated along the circle for five laps. At the end of each trial, the robot's estimated position and orientation, as estimated by the odometry system, were recorded. The results of these tests are in Table 6.2. Since the start and end positions are the same, perfect localization would have observed the robot to be at $x = 0.0$ meters and $y = 0.0$ meters with a heading of 0. The results show that turning has a more negative effect on odometry accuracy than driving in a straight line. The displacement was consistently incorrect by at least 0.8 meters, and the heading was incorrect by up to 35 degrees. The consistent bias in these errors (they always have the same sign) can be explained by the fact that the robot was driven around the circle in the same direction (counterclockwise) in every trial.

As expected, change in heading causes a greater error in the odometric localization. The greater error due to change in heading is a feature of the differential drive system on ABBY. For a differential drive system to turn, one or both wheels must slip, which introduces error into the odometry. The results of these odometry trials show that although the odometry is relatively accurate for short distances, it accumulates

Table 6.2: One meter radius circle odometry test

Trial	x	y	O_z	O_w	Displacement	Heading (deg)
1	0.730	0.432	0.507	0.862	0.849	29.124
2	0.802	0.45	0.528	0.849	0.920	26.202
3	0.941	0.596	0.613	0.790	1.114	14.370
4	0.751	0.621	0.558	0.830	0.974	22.150
5	0.778	0.330	0.459	0.889	0.845	35.404
6	0.892	0.434	0.502	0.865	0.992	29.677
RMS	0.819	0.488	0.530	0.848	0.954	26.975
STD	0.0833	0.111	0.053	0.034	0.101	7.235

Measurements in meters except where noted. O_z and O_w indicate quaternion components z and w (components x and y are 0).

large error as greater distance is traveled, particularly in the heading estimate and particularly when the robot is turned. This error is effectively canceled out by AMCL.

6.2 Validation Tasks

In order to validate the basic functionality of the robot, three simple tasks were devised to verify the performance of the drive base, the manipulation system, and the whole robot.

To validate the drive base, the robot was scripted to drive from one of two starting positions (designated “left” and “right”) to a table at a predefined location, then drive to a predefined final destination. This task tests the localization and navigation systems. Between each trial, the robot’s position estimate was reset, and AMCL was reseeded with a rough estimate of the appropriate starting position. Success was defined as traveling directly to the table without colliding with anything in the room, then driving directly to the final position, again without colliding with anything. The results of these tests are shown in Table 6.3.

In several trials, the robot spun one or more times before settling into the final

position. In one trial (16), the robot failed to settle into the goal position during this spin because it was stopped when the gripper brushed an obstacle. The cause of this behavior is unknown, but the drive base planners were observed to be running slower than the desired rate due to the heavy load on the PC’s CPU. It is possible that this caused the robot to overshoot the desired heading and perform a full rotation.

Table 6.3: Results of drive base validation tests

Trial	Start Position	Drive To Table	Drive to Final Position
1	Left	Successful	Several spins at goal position before success
2	Left	Successful	Several spins at goal position before success
3	Left	Successful	Successful
4	Left	Successful	Successful
5	Left	Successful	Successful
6	Left	Successful	Successful
7	Left	Successful	Successful
8	Left	Successful	Several spins at goal position before success
9	Right	Successful	Successful
10	Right	Successful	Successful
11	Right	Successful	Successful
12	Right	Successful	Successful
13	Right	Successful	Successful
14	Right	Successful	Successful
15	Right	Successful	Successful

16	Right	Successful	Arrives at goal position, then spins several times and the gripper brushes an obstacle
----	-------	------------	--

In order to validate the object recognition and manipulation system, the robot was scripted to pick up one of three objects placed randomly within a designated area on a table in front of the robot. The robot used the tabletop segmentation and object recognition software described in Section 4.4 above to locate the objects on the table, pick one up, and drop it in the onboard carrier bin. The objects, 5 cm diameter by 5.5 cm tall paper cylinders, were only slightly smaller than the gripper, which has a jaw opening of 5.3 cm when opened. Smaller (4.5 cm diameter) cylinders were also tested, but they were too small to be reliably located with the Kinect.

Each trial began with the robot approaching the table with the arm stowed. During the approach, the Kinect had an unobscured view of the whole table, allowing the robot to add the table to the collision map. Once the robot arrived at the table, it moved its arm to the side to maximize the Kinect's view of the table. Once the arm was out of the way, the robot attempted object segmentation. If no objects were found, the robot moved the arm again and reattempted segmentation. If at least one object was recognized, the robot attempted to pick one up and drop it in the bin. The results of these tests are shown in Figure 6.1 and Table 6.4.

Of the twenty-five trials, the robot completed the manipulation task thirteen times. In three attempts, the gripper missed the object, resulting in a failed pick. These failures can be attributed to the very small clearance between the 5 cm object and the 5.3 cm gripper jaw. In one of the trials (15), two objects were obscured from the Kinect by the robot arm and the third was not reachable by the robot's arm. The most common cause of failure was the robot gripper making contact with the table. This problem caused six trials to fail. The ROS arm navigation software used on the robot is configured to generate collision-free arm trajectories, as described in Section 4.3 above, but for an unknown reason, it does not always do so. A proposed solution,

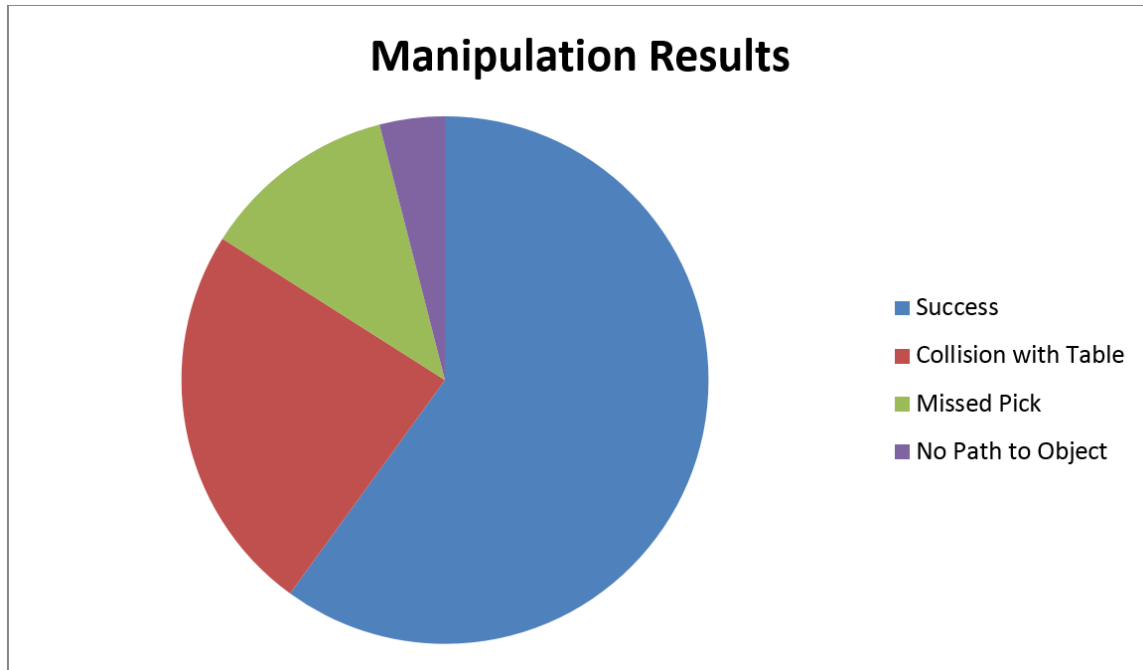


Figure 6.1: Manipulation test results

using recently released ROS software, is proposed in Chapter 8 below.

Table 6.4: Results of object recognition and manipulation tests

1	3	Success	Success
2	3	Success	Success
3	3	Success	Success
4	2	Success (3 rd attempt)	Success
5	2	Missed (gripper nudges table)	Success (with no object)
6	2	Success (2 nd attempt)	Success
7	3	Success	Success
8	4	Success (2 nd attempt)	Success
9	2	Success, insecure grip (3 rd attempt)	Success (object fell)
10	3	Missed	Success (with no object)
11	2	Missed	Success (with no object)
12	2	Success	Success

Trial	Objects Recognized	Pick Result	Drop Result
13	2	Missed (gripper nudges table)	Success (with no object)
14	2	Success (2 nd attempt)	Success
15	1	Cannot find a path to the object	N/A
16	2	Gripper hits table	N/A
17	2	Gripper hits table	N/A
18	2	Success	Success
19	3	Success	Success
20	2	Gripper hits table	N/A
21	1	Success, insecure grip (3 rd attempt)	Success (object fell)
22	2	Success	Success (takes over 60 s)
23	2	Gripper hits table	N/A
24	3	Success	Success
25	2	Missed	Success (with no object)

Finally, these tests were combined into a single procedure that simulates part of the task of retrieving an assembly kit from factory inventory. The procedure is as follows:

1. Beginning at one of two starting locations, drive to a predetermined location near a table a few meters away.
2. Locate at least one of three small manipulable objects on the table using the Kinect.
3. Lift one of the target objects from the table.
4. Place the target object in the onboard carrier bin.
5. Drive to the final destination.

This task is meant to simulate the act of driving through a factory to a shelf (represented by the table), picking up an item for a kit, and delivering it to the assembly station. In an actual factory environment, steps 1 through 4 would be performed repeatedly until every item in the kit was retrieved.

The driving portions of the task test the drive base hardware and software, including the localization and navigation systems. The object recognition portion of the task tests the Kinect and the tabletop perception software. The manipulation portions of the task test the arm hardware and the arm navigation stack, including the inverse kinematic solver, path planner, and collision environment monitor.

The task described was performed by the robot eight times. The robot started from one of two locations, designated "left" and "right", which were marked on the floor of the testing area. Between each trial, the target objects were placed randomly within a designated area on the table and the robot's localization software was reinitialized, with AMCL seeded at the appropriate starting location. Of the eight trials performed, seven were considered successful. Table 6.5 shows these results.

Table 6.5: Validation Task Results

1	Left	2	Robot spins before settling into final position
2	Left	2	Gripper brushes table and knocks over 1 object; robot spins before settling into final position
3	Left	N/A	Robot approaches table, but get stuck in spin
4	Left	1	Object recognition/pickup succeeds on fourth attempt
5	Right	1	Low batteries prevent robot from aligning in final position

Trial	Start Position	Objects Recognized	Notes
6	Right	2	
7	Right	1	Low batteries prevent robot from aligning in final position
8	Right	3	Robot spins before settling into final position

Of the seven successful trials, most exhibit a similar behavior at the end of the trial. The robot spins one or more times before settling into the final position. This behavior (at the table, rather than the final position) was also the cause of the single failed trial. The cause of this behavior is unknown, but the drive base planners were observed to be running slower than the desired rate due to the heavy load on the PC's CPU. It is possible that this caused the robot to overshoot the desired heading, causing it to perform a full rotation. Whereas the robot eventually recovered from this problem at the final position, it could not recover at the table because of the tight tolerance required to approach so close to the table.

6.3 Battery Performance

Three tests were performed to determine the life of the battery. In each test, the test process was run until the battery voltage reached 21.5 volts DC, which was considered the critical shutdown voltage. At this point, each cell in the lead acid battery has been depleted to about 1.8 volts, or 90% of its nominal voltage.

In the first test, the robot's systems are all turned on, but the actuators are disabled. In this idle test, the robot ran for 4 hours and 44 minutes before it hit the critical voltage.

In the second test, the robot was strapped to a platform with rollers, and the

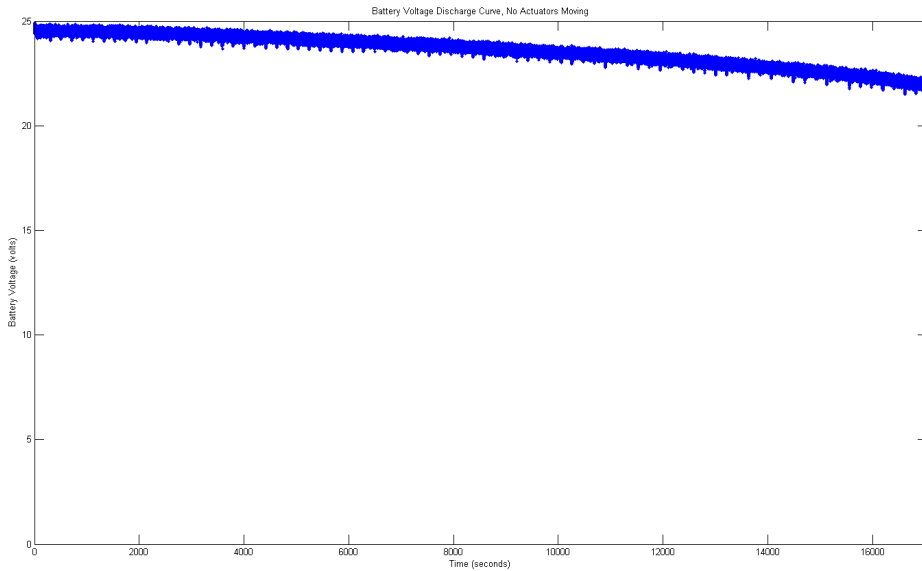


Figure 6.2: Voltage curve during battery discharge test with actuators idle

drivetrain was exercised by commanding rotational velocities that followed a sawtooth profile, increasing from the maximum negative velocity to the maximum positive velocity, then resetting back to the maximum negative velocity. In this test, the robot ran for 3 hours and 13 minutes before it hit the critical voltage.

In the third test, the drivetrain was disabled but the arm was commanded to repeatedly execute trajectories between the stow position and the position to drop an object in the bin. At the end of each trajectory, the gripper was opened or closed. In this test, the robot ran for only 36 minutes. These results indicate that the arm consumes significantly more power than other components of the robot.

These tests indicate that the robot could run in typical operation for about one hour before its batteries are critically low.

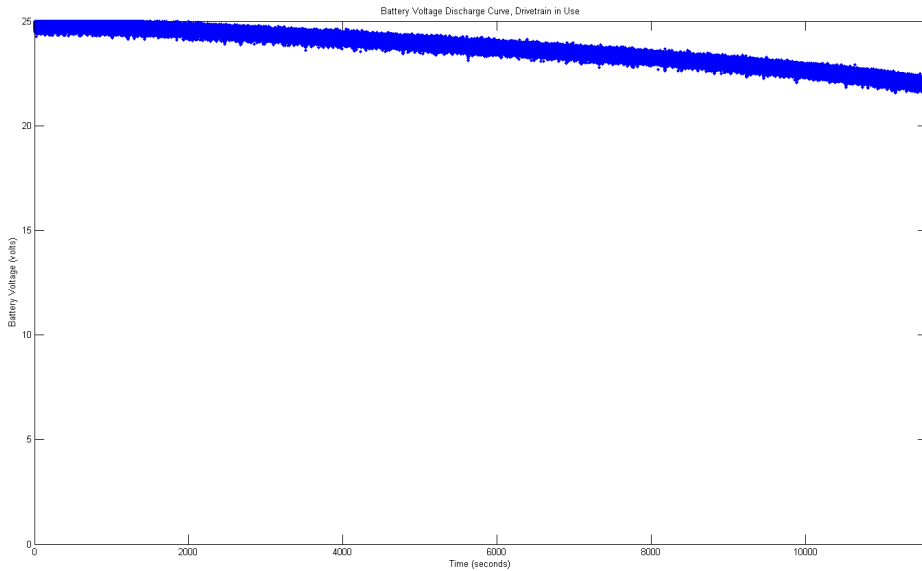


Figure 6.3: Voltage curve during battery discharge test with drivetrain exercised

6.4 The Kinect

6.4.1 For Object Localization and Arm Planning

A major part of the validation task depended on the Kinect as a sensor for object segmentation and recognition. The Kinect point cloud was used as the input to segmentation and localization nodes to determine the location of manipulable objects on a table. Although the Kinect has been shown to have some warping[32], it proved adequate to recognize the small cylindrical objects used for the validation task. Two different Kinects were tested on this robot. The first Kinect used was improperly calibrated, and its color data was very badly registered to its depth data. It is unknown whether this is caused by a factory defect or damage during use. The second Kinect tested did not exhibit these problems and was successfully used to localize objects in the validation task.

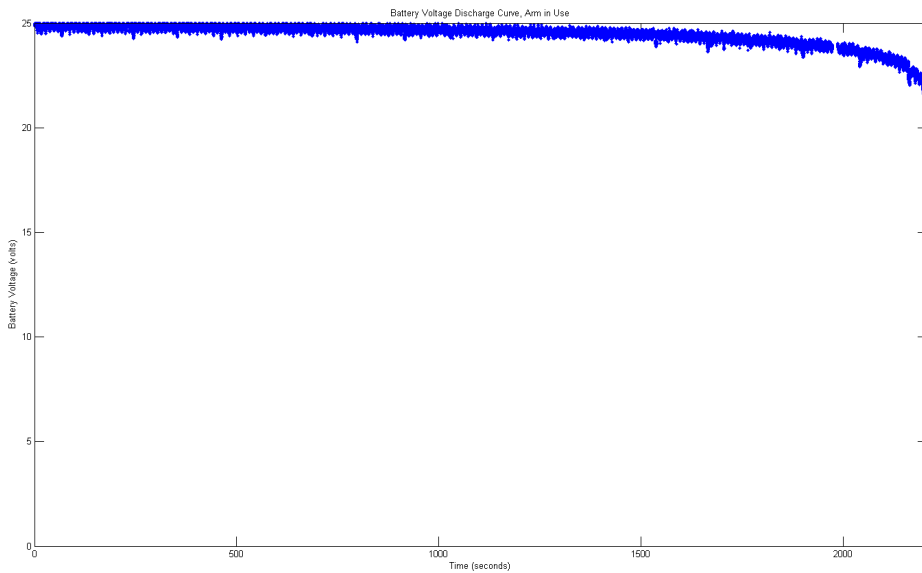


Figure 6.4: Voltage curve during battery discharge test with arm exercised

6.4.2 For Reading QR Codes

The Kinect’s RGB camera captures video at VGA resolution (640 by 480 pixels). Experiments with reading QR codes showed that a Kinect did not have sufficient resolution to read a tag, even when the tag filled the entire field of view of the Kinect. This means that in order for the Kinect to be useful for recognition of tagged “smart” payloads, it must be paired with (and calibrated to) an external camera with a higher resolution sensor.

Chapter 7

Conclusion

The lack of cheap, robust mobile manipulators has prevented manufacturers from adopting them and has hampered research into mobile manipulation. ABBY, being both cheap and robust, fills the needs of both groups. With a total component cost less than \$40,000, this platform is significantly cheaper than existing mobile manipulation platforms. This savings in cost was in large part due to the use of mass-produced hardware components. The hardware platform is constructed of industrial and commercial components. These components have been rigorously tested by their manufacturers and in the field. As a result, the hardware is more durable than experimental “research-grade” hardware, which is not subject to the quality controls of mass-produced products. These hardware components were successfully integrated into a system capable of traversing indoor environments and manipulating small objects.

In addition to a robust hardware platform, existing software from the ROS community was integrated to create a capable robot. ABBY is able to navigate indoor environments with *a priori* maps using a combination of relative and global localization and a ROS-standard planner. Using ROS software adapted to this platform, ABBY can locate objects on a table using a Kinect camera. A software driver for

ABB industrial robotic arms was created specifically for this project and contributed to the ROS Industrial project. Using this software, ABBY can pick up recognized objects and store them in an onboard carrying bin. The software on ABBY is modular, using existing ROS frameworks and APIs wherever possible. The use of a modular software system will enable future researchers to easily augment the system with new experimental software.

Overall, the robot shows promising initial results. In sixteen trials of the mobile base, fifteen were complete successes. Of twenty-five trials of the manipulation system, fifteen were successes. The limited range of the gripper calls for precise object localization, which was nonetheless achieved with the Kinect in the majority of trials. The biggest problem with the manipulation system was unreliable collision checking. Development of collision checking software was beyond the scope of this project, and this is an area of future research. In combined mobile manipulation trials, the robot performed its task perfectly in seven out of eight trials. These results show that the robot's hardware and software systems are reliable enough to make it a useful research platform, demonstrating that a mobile manipulator can be created for much lower cost than currently available platforms.

This robot was designed for experiments with kitting operations in a factory environment. However, the platform is useful for other applications as well. Researchers at other institutions have used mobile manipulators for household tasks, and this platform could be used for similar research. This research could also dovetail with previous work at Case into assistive robots for the disabled. By providing a low-cost platform for mobile manipulation research, this robot enables researchers to tackle these and other problems without the significant expense of other mobile manipulators.

This robot, with upgrades to its end effector, would also be an effective mobile manufacturing platform. Rather than having to build and rebuild a fixed manufactur-

ing cell for each change in production requirements, industrial engineers could design rapidly reconfigurable assembly lines composed of one or more mobile manipulators. These systems would also allow rapid set-up of small manufacturing operations at new manufacturing sites and remote locations such as construction sites or in space.

Chapter 8

Future Work

Although this platform is now functional and useful for research, there are several areas in which future researchers could improve it.

The biggest problem with the manipulation subsystem is that the ROS arm navigation software sometimes generates trajectories that result in collisions with furniture in the robot's environment. The cause of this problem is unknown. Future researchers should evaluate alternative ROS-compatible collision checkers.

The current power system only allows about one hour of operation before recharging the batteries. The ability to charge or change the batteries autonomously would make the robot more useful.

There are two promising avenues of exploration to reduce the cost of the platform. The cRIO and auxiliary hardware used to control the mobile base (breakout boards and speed controllers) account for over 10% of the overall system cost. Future researchers should explore newer, more affordable alternatives to reduce the cost of the system without compromising its capabilities. The SICK LIDAR accounts for over 15% of the overall system cost. Future researchers should evaluate other ranging sensors to determine if there is a more affordable alternative that is sufficiently accurate and robust for this platform.

Evaluation and integration of more sensors could allow the robot to perform more functions than it can now. The Kinect is a low-resolution (VGA) camera, and one of the key future goals of this project is to be able to identify manipulable objects from bar codes or QR codes. A higher resolution camera (perhaps mounted on the robot's manipulator) could be used to examine objects to be picked up. Because the robot has no rear-facing sensors, it cannot safely back up, and SLAM algorithms fail when the robot drives through doorways. Adding rear-facing sensors would allow the robot to safely back up and might also solve the problems that prevented the use of SLAM for absolute localization.

The two-position parallel plate gripper used for this project was simple and readily available, but it limits the robot to being able to manipulate boxes in a limited range of sizes. Future researchers should explore different types of grippers and evaluate their cost effectiveness and performance in this robot's intended application.

Over the course of the project, several problems were identified with ROS stability. For ROS software to be a viable option in an industrial environment, it must be meticulously tested and shown to be robust, secure, and safe. Currently, most software outside of the ROS core does not meet these requirements. Testing more ROS packages and improving their stability would be a boon to the open source robotics community and to the industrial robotics industry.

As described above, the current emergency stop system is incomplete and relies on a tethered emergency stop button. A revised emergency stop design, described in Appendix 2, was created as part of this thesis, but has not yet been constructed and installed on the platform.

As described above, the robot currently operates at low speed so that a reflexive speed limiting system is not necessary. Adding reflexive speed limiting to the robot would allow high speed operation without compromising safety. Some proposed speed limiting systems are described in Appendix 3.

Appendix A

Bill of Materials

Table A.1: Bill of Materials

Wheelchair Base	\$3000
Batteries	\$400
Chassis Frame Materials	\$1000
LIDAR	\$6000
IRB-120/IRC5	\$23000
cRIO 9074	\$4150
+ 9403 DIO module	
+9401 DIO module	
+ 9201 analog input module	
PC Case	Total \$65 \$547
Power Supply	\$90
Solid State Hard Drive	\$50
Motherboard	\$70
Processor	\$230
RAM	\$42
Kinect	\$150

APPENDIX A. BILL OF MATERIALS

Item	Cost
Grayhill Encoder (4)	\$320
13.8 v Regulator	\$81
I/O Breakout Board	\$45
Emergency Stop System	\$160
AC Inverter	\$322
Sabertooth 2x50	\$250
Compressor	\$250
Network Equipment	\$40
RS-422 – USB converter	\$80
Arduino	\$30
Miscellaneous Electrical Components	\$50
Total	\$1778.00

Appendix B

Revised Emergency Stop Design

A revised version of the emergency stop circuit was designed and portions of it prototyped, but it has not been tested. This version should fix the problems discovered in the first version of the emergency stop.

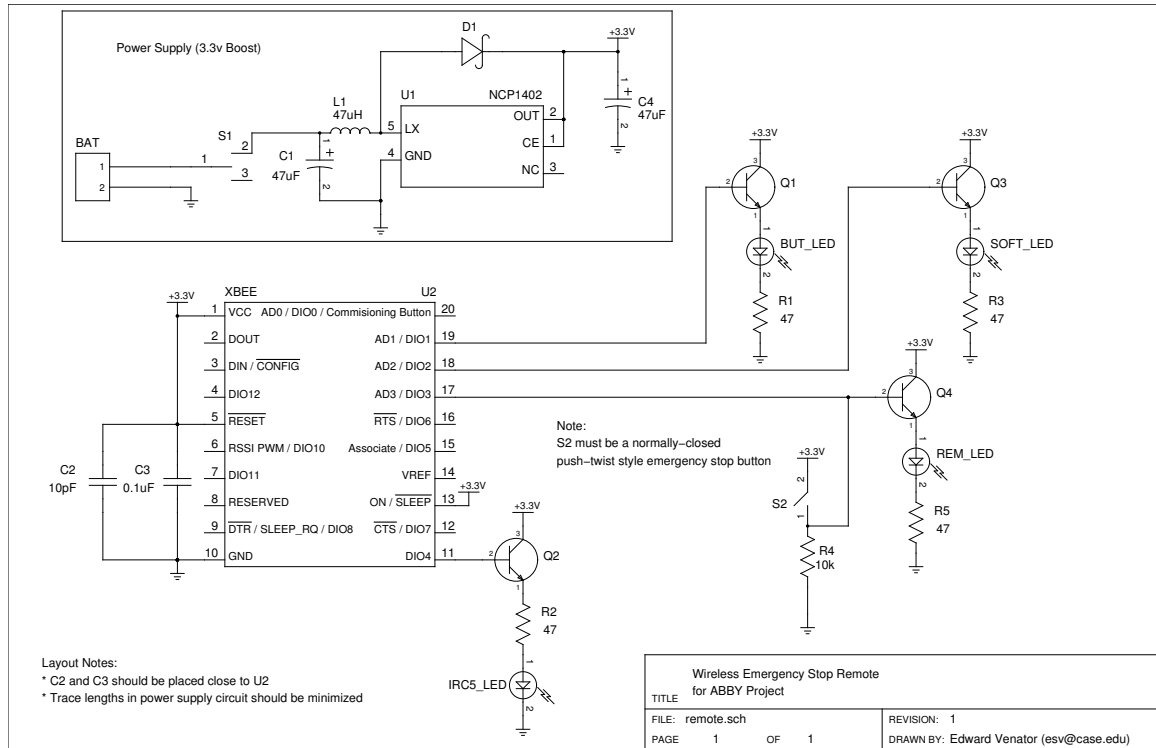


Figure B.1: Revised emergency stop remote circuit.

To allow the system to stop the IRC5, the optoisolator on the output of the

emergency stop circuit was replaced with a relay module, which will more reliably switch the General Stop input of the IRC5. To complete integration with the IRC5, the RAPID software must be modified to output the current General Stop state to a GPIO, which should be connected to the IRC5 input of the emergency stop circuit.

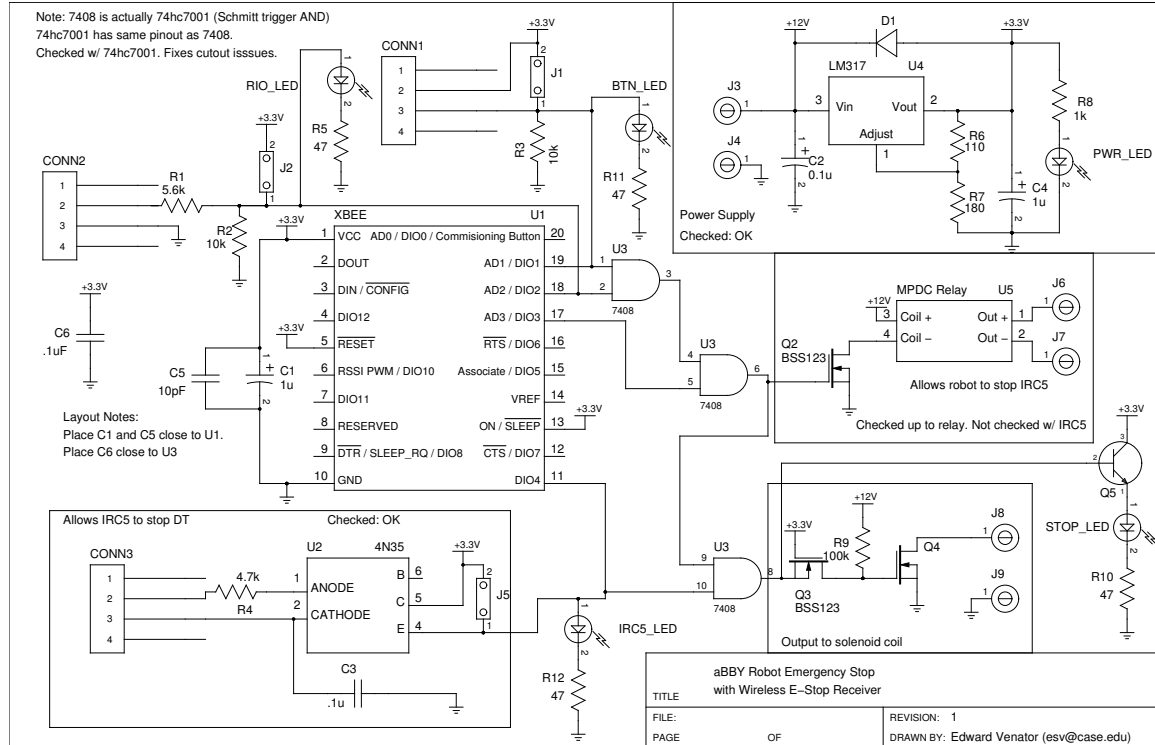


Figure B.2: Revised emergency stop receiver/aggregator circuit.

To solve the wireless communication issues, the power supply in the remote was replaced with a 3.3 volt regulated boost supply, which should be much more reliable, and bypass capacitors were added to the power rails of the XBee modules on both the remote and the emergency stop circuit. Testing has shown that the XBee modules are reliable when a sufficiently clean and reliable DC supply is available to power them.

In addition to solving the problems described above, some small changes were made to improve the circuit. To reduce the power consumption of the emergency stop circuit and reduce the heat produced by the onboard power regulator, the Darlington transistor used to switch the coil of the drivebase enable solenoid was replaced with a MOSFET circuit that performs the same function. To make the system easier to

use and more reliable, the momentary switch and latch used on the previous version was replaced with a twist-lock style emergency stop switch.

Although this system has not been constructed, its constituent parts have been tested individually. The MOSFET switching circuit has been confirmed to work with a resistive load equivalent to the coil resistance of the solenoid used to switch the drive base power rail. The power supply circuit in the remote has been tested and provides a reliable 3.3 volt power supply from a pair of AA batteries. The use of a relay instead of a transistor to control the General Stop input is in line with recommendations from ABB's documentation, and the relay used meets the requirements. If the necessary components can be acquired for this emergency stop circuit, it should be able to meet all of the requirements described above.

Appendix C

Reflexive Collision Avoidance

As described in Section 5.1, ABBY is slow enough that it can be operated safely without a reflexive speed limiting system. This appendix describes proposed speed limiting systems to allow the robot to be operated more quickly.

C.1 Reflexive Halt Methods for Mobile Bases

ABBY’s local planner will not allow for collisions with obstacles seen by the LIDAR, and it updates velocity commands at 12 Hz. Although this is sufficiently safe for testing, a more robust solution would be necessary in an industrial setting. Mobile robots often implement a reflexive halt as shown in Algorithm 3. For example, if a measurement source such as a LIDAR reports that there is an obstacle in front of the robot at close range, the robot’s velocity would be limited to turning and reversing. This approach is effective, but can cause difficulties in navigating tight areas, where there may be enough space for a robot to navigate through obstacles if it does so carefully.

Another approach to reflexive halting was described by Chad Rockey in his masters thesis [32]. This approach, called Reflexive Avoidance Plus, was developed for a smart wheelchair, which must operate in crowded areas around people. Reflex-

Algorithm 3 A simple reflexive halt algorithm. If an obstacle is close to the robot, the robot is prevented from approaching closer.

```
Given: Sensor measurements  $M$ 
for all measurement  $m$  in  $M$  do
    if dangerous( $m$ ) then
        prevent motion in direction of  $m$ 
    end if
end for
```

ive Avoidance Plus uses velocity limiting rather than preventing motion altogether. When a sensor detects an obstacle in the robot's path, it limits the maximum velocity in that direction using a scaling function based on the distance of the obstacle from the robot. This approach prevents the robot from colliding with an obstacle (the maximum velocity is zero below a certain threshold distance), but allows low speed progress toward an obstacle. Because the robot approaches the obstacle at lower speed, it can safely get closer to obstacles.

Since the Reflexive Avoidance Plus method described by Rockey was implemented on a robotic platform of similar size and speed to this robot, it would be a good candidate for this robot. However, there is some work still to be done to adapt the code, which was designed specifically for the wheelchair, to ABBY.

C.2 Reflexive Halting for Manipulators

In addition to the mobile base, ABBY's robotic arm poses a risk for collisions. In industrial situations, manipulators are kept inside safety cages to prevent people from interfering with them or getting injured. A safety cage is not a possibility for a mobile manipulator, so another solution is necessary. A reflexive halt for the manipulator allows it to operate safely in the presence of people and obstacles without a safety cage.

Like the mobile base planner, the planner for the arm generates collision-free paths. However, the planner for the arm does not replan at all once it commits to

a trajectory. The trajectory is generated and sent to the IRC5 for execution, and then ROS waits for the trajectory to be executed. If something enters the path of the trajectory, the robot does not alter the current trajectory. This makes the robot unsafe to operate around humans above a certain joint speed.

Rethink Robotics, with their robot Baxter [33], solved the problem of operating an industrial robot without a safety cage with a mechanical and software solution that relied on force feedback and serial-elastic actuators. Because all of Baxter’s joints are elastic and its arms are so light, it can safely collide with people and obstacles. It also uses force feedback in its joints to detect these collisions and become passive, allowing people to push it around. Because ABBY’s robotic arm does not have serial elastic actuators or force feedback in the joints, this solution is not possible.

Using the Kinect sensor, it would be possible to implement one of several possible reflexive collision avoidance methods on ABBY. One method would be to halt arm motion when an obstacle enters the arm’s work envelope and suspend arm motion until the obstacle leaves the work envelope. Although this is arguably the safest solution, it can cause the robot to become stuck in the stopped state. If an inanimate obstacle is brought into the robot’s work envelope and left there, the robot will never re-enable the arm.

To resolve this problem, the reflexive halt behavior can be augmented as shown in Algorithm 4. In this algorithm, the currently planned path is repeatedly checked for dangerously close objects (such as people) until execution is completed. If an object enters the dangerous area, the robot stops execution of the trajectory and waits. If the obstacle leaves the area before a timeout is reached, the robot resumes execution of the trajectory. If the obstacle does not move, the robot will attempt to retry planning to move around the obstacle to accomplish its goal. This reflexive halt algorithm has two advantages over the naive algorithm described in the previous paragraph. First, it does not stop for obstacles that enter the work envelope but do

not interfere with the planned motion. This allows humans to work alongside the robot and interact with it by giving it objects or taking objects from it. Second, it will plan around stationary objects that enter the work envelope, allowing a person to leave an object in the work envelope without stalling the robot.

Algorithm 4 An algorithm for reflexive halting for a mobile manipulator. If an obstacle enters the manipulation path, the robot waits, then replans.

```
Given: Current Plan  $P$ , Measurements  $M$ 
for all state  $s$  in  $P$  do
    for all measurement  $m$  in  $M$  do
        if dangerous( $m, s$ ) then
            halt
            wait for obstacle to move or replan
        end if
    end for
end for
```

The National Institute for Standards and Tests (NIST) has developed an algorithm to determine a safe separation distance S for a human to approach a robot. This is described in Equation C.1 below, where K_H is the speed of a moving human, K_R is the speed of the robot, T_R is the reaction time of the human, T_B is the braking time of the robot, B is the robot braking distance, and C is a distance to account for measurement uncertainty [34].

$$S = K_H * (T_R + T_B) + K_R * T_R + B + C \quad (\text{C.1})$$

NIST researchers used this equation, LIDAR scanners, and a Kalman filter to track humans moving through the robot's work envelope and determine whether a human had entered a danger zone around the robot (if the distance from the robot to the human is less than S). This method completes Algorithm 4 by filling in the dangerous() function. In order to implement this algorithm on ABBY, parameters B and C would first have to be determined for this platform. Then, the algorithm would have to be written as a ROS node and tested on this robot.

Bibliography

- [1] H. Barbera, J. Quinonero, M. Izquierdo, and A. Skarmeta, “i-Fork: a flexible AGV system using topological and grid maps,” in *IEEE International Conference on Robotics and Automation (ICRA)*, vol. 2, 2003, pp. 2147–2152 vol.2.
- [2] K. Vivaldini, J. P. M. Galdames, T. Bueno, R. Arajo, R. Sobral, M. Becker, and G. A. P. Caurin, “Robotic forklifts for intelligent warehouses: Routing, path planning, and auto-localization,” in *2010 IEEE International Conference on Industrial Technology (ICIT)*, 2010, pp. 1463–1468.
- [3] G. Garibotto, S. Masciangelo, P. Bassino, C. Coelho, A. Pavan, and M. Marson, “Industrial exploitation of computer vision in logistic automation: autonomous control of an intelligent forklift truck,” in *1998 IEEE International Conference on Robotics and Automation*, vol. 2, 1998, pp. 1459–1464 vol.2.
- [4] “Kiva vs. Automated Guided Vehicles.” [Online]. Available: [http://www.kivasytems.com/solutions/kiva-vs-traditional/
solutionskiva-vs-traditionalkiva-vs-agvs/](http://www.kivasytems.com/solutions/kiva-vs-traditional/solutionskiva-vs-traditionalkiva-vs-agvs/)
- [5] R. D’Andrea and P. Wurman, “Future challenges of coordinating hundreds of autonomous vehicles in distribution facilities,” in *IEEE International Conference on Technologies for Practical Robot Applications (TePRA)*, Nov., pp. 80–83.

- [6] R. Bischoff, U. Huggenberger, and E. Prassler, “KUKA youBot - a mobile manipulator for research and education,” in *2011 IEEE International Conference on Robotics and Automation (ICRA)*, May, pp. 1–4.
- [7] C. Cosma, M. Confente, M. Governo, and P. Fiorini, “An autonomous robot for indoor light logistics,” in *2004 IEEE/RSJ International Conference on Intelligent Robots and Systems, 2004. (IROS 2004). Proceedings*, vol. 3, Oct., pp. 3003–3008 vol.3.
- [8] A. Hermann, Z. Xue, S. Ruhl, and R. Dillmann, “Hardware and software architecture of a bimanual mobile manipulator for industrial application,” in *2011 IEEE International Conference on Robotics and Biomimetics (ROBIO)*, Dec., pp. 2282–2288.
- [9] E. Venator, Gregory Lee, and W. Newman, “Hardware and Software Architecture of ABBY: An Industrial Mobile Manipulator,” Madison, WI, USA, Aug. 2013.
- [10] A. B. B. Robotics, “IRB-120 Industrial Robot,” May 2012. [Online]. Available: [http://www05.abb.com/global/scot/scot241.nsf/veritydisplay/3bd625bab3c7cae1c1257a0800495fac/\\$file/ROB0149EN_D_LR.pdf](http://www05.abb.com/global/scot/scot241.nsf/veritydisplay/3bd625bab3c7cae1c1257a0800495fac/$file/ROB0149EN_D_LR.pdf)
- [11] S. America, “DC-DC Step Down Converters Model SDC-15.” [Online]. Available: <http://www.samlexamerica.com/documents/product-specs/SDC-15-Samlex-Specifications.pdf>
- [12] Eric Perko, “Precision Navigation for Indoor Mobile Robots,” Masters, Case Western Reserve University, Cleveland, OH, Jan. 2013.
- [13] “ROS/Concepts - ROS Wiki.” [Online]. Available: <http://www.ros.org/wiki/ROS/Concepts>
- [14] “actionlib - ROS Wiki.” [Online]. Available: <http://www.ros.org/wiki/actionlib>

- [15] “openni_kinect - ROS Wiki.” [Online]. Available: http://www.ros.org/wiki/openni_kinect
- [16] “laser_drivers - ROS Wiki.” [Online]. Available: http://www.ros.org/wiki/laser_drivers?distro=fuerte
- [17] C. Rockey, E. Perko, and Ben Ballard, “HARLIE,” IGVC, Tech. Rep., May 2010. [Online]. Available: <http://www.igvc.org/design/2010/CWRU-Harlie.pdf>
- [18] E. Venator, “Rosserial Service ”Failed to parse subscriber” - ROS Answers.” [Online]. Available: <http://answers.ros.org/question/48548/rosserial-service-failed-to-parse-subscriber/>
- [19] ——, “rosserial.” [Online]. Available: <https://github.com/evenator/rosserial>
- [20] Shaun Edwards and Chris Lewis, “ROS-Industrial Applying the Robot Operating System (ROS) to Industrial Applications.” St. Paul, Minnesota, USA: IEEE, May 2012.
- [21] S. Thrun, W. Burgard, and D. Fox, *Probabilistic Robotics*. The MIT Press, Aug. 2005.
- [22] G. Grisetti, C. Stachness, and W. Burgard, “Gmapping.” [Online]. Available: <http://www.Openslam.org/gmapping.html>
- [23] Tony Yanick, Chase Nemeth, Beom Koh, and Avinash Karamchandani, “ALEN,” IGVC, Tech. Rep., 2009. [Online]. Available: <http://www.igvc.org/design/2009/Case%20Western%20Reserve%20University%20-%20Alen.pdf>
- [24] “navfn - ROS Wiki.” [Online]. Available: <http://www.ros.org/wiki/navfn>
- [25] E. W. Dijkstra, “A note on two problems in connexion with graphs,” *Numerische Mathematik*, vol. 1, no. 1, pp. 269–271, Dec. 1959. [Online]. Available: <http://link.springer.com/article/10.1007/BF01386390>

- [26] “Kinematic and Dynamic Solvers | The Orocovis Project.” [Online]. Available: http://www.orocos.org/kdl/UserManual/kinematic_solvers
- [27] “OpenRAVE | ikfast Module | OpenRAVE Documentation.” [Online]. Available: http://openrave.org/docs/latest_stable/openravepy/ikfast/#ikfast-the-robot-kinematics-compiler
- [28] G. Snchez and J.-C. Latombe, “A Single-Query Bi-Directional Probabilistic Roadmap Planner with Lazy Collision Checking,” in *Robotics Research*, ser. Springer Tracts in Advanced Robotics, P. R. A. Jarvis and P. A. Zelinsky, Eds. Springer Berlin Heidelberg, Jan. 2003, no. 6, pp. 403–417. [Online]. Available: http://link.springer.com/chapter/10.1007/3-540-36460-9_27
- [29] “tabletop_object_detector - ROS Wiki.” [Online]. Available: http://www.ros.org/wiki/tabletop_object_detector
- [30] M. A. Fischler and R. C. Bolles, “Random Sample Consensus: A Paradigm for Model Fitting with Applications to Image Analysis and Automated Cartography,” AI Center, SRI International, 333 Ravenswood Ave., Menlo Park, CA 94025, Tech. Rep. 213, Mar. 1980.
- [31] “QR code,” Mar. 2013, page Version ID: 546110040. [Online]. Available: http://en.wikipedia.org/w/index.php?title=QR_code&oldid=546110040
- [32] Chad Rockey, “Low-Cost Sensor Package for Smart Wheelchair Obstacle Avoidance,” Masters, Case Western Reserve University, Cleveland, OH, Jan. 2012.
- [33] “baxter.” [Online]. Available: <http://www.rethinkrobotics.com/baxter/>
- [34] W. Shackleford, R. Norcross, J. Marvel, and S. Szabo, “Integrating occlusion monitoring into human tracking for robot speed and separation monitoring,” in *Proceedings of the Workshop on Performance Metrics for Intelligent Systems*,

ser. PerMIS '12. New York, NY, USA: ACM, 2012, pp. 168–173. [Online]. Available: <http://doi.acm.org/10.1145/2393091.2393124>